Multi-proxy record of ocean-climate variability during the last two millennia on the Mackenzie Shelf, Beaufort Sea

Laura Gemery[1,2], Thomas M. Cronin[1], Lee W. Cooper[2], Lucy R. Roberts[3],
Lloyd D. Keigwin[4], Jason A. Addison[5], Melanie J. Leng[6,7], Peigen Lin[8], Cédric Magen[9],
Marci E. Marot[10] and Valerie Schwartz[5]

[1]U.S. Geological Survey, Florence Bascom Geoscience Center, Reston, VA 20192, USA
[2]Chesapeake Biological Laboratory, University of Maryland Center for Environmental Sciences, Solomons, MD 20688
email: cooper@umces.edu
[3]Department of Ecoscience, Aarhus University, C. F. Møllers Allé 4-5, 8000 Aarhus, Denmark
email: l.roberts@ecos.au.dk
[4]Department of Geology and Geophysics, Woods Hole Oceanographic Institution, Woods Hole, MA 02543, USA
email: lkeigwin@whoi.edu
[5]U.S. Geological Survey, Geology, Minerals, Energy, and Geophysics Science Center, Menlo Park, CA 94025, USA
email: jaddison@usgs.gov; vberson22@gmail.com
[6]National Environmental Isotope Facility, British Geological Survey, Keyworth, Nottingham, NG12 5GG, United Kingdom
email: mjl@bgs.ac.uk
[7]Centre for Environmental Geochemistry, School of Biosciences, University of Nottingham,
Sutton Bonington Campus, Loughborough LE12 5RD, United Kingdom
[8]Department of Physical Oceanography, Woods Hole Oceanographic Institution, Woods Hole, MA 02543, USA
email: plin@whoi.edu
[9]University of Maryland, Department of Geology, College Park, MD 20742
email: cmagen@umd.edu
[10]U.S. Geological Survey, St. Petersburg Coastal and Marine Science Center,
600 4th Street South, St. Petersburg, FL 33701, USA
email: mmarot@usgs.gov
Corresponding author: Laura Gemery, lgemery@usgs.gov

————————

ABSTRACT: A 2,000 year-long oceanographic history, in sub-centennial resolution, from a Canadian Beaufort Sea continental shelf site (60 meters water depth) near the Mackenzie River outlet is reconstructed from ostracode and foraminifera faunal assemblages, shell stable isotopes (δ^{18}O, δ^{13}C) and sediment biogenic silica. The chronology of three sediment cores making up the composite section was established using ^{137}Cs and ^{210}Pb dating for the most recent 150 years and combined with linear interpolation of radiocarbon dates from bivalve shells and foraminifera tests. Continuous centimeter-sampling of the multicore and high-resolution sampling of a gravity and piston core yielded a time-averaged faunal record of every ~40 years from 0 to 1850 CE and every ~24 years from 1850 to 2013 CE. Proxy records were consistent with temperature oscillations and related changes in organic carbon cycling associated with the Medieval Climate Anomaly (MCA) and the Little Ice Age (LIA). Abundance changes in dominant microfossil species, such as the ostracode *Paracyprideis pseudopunctillata* and agglutinated foraminifers *Spiroplectammina biformis* and *S. earlandi*, are used as indicators of less saline, and possibly corrosive/turbid bottom conditions associated with the MCA (~800–1200 CE) and the most recent ~60 years (1950–2013). During these periods, pronounced fluctuations in these species suggest that prolonged seasonal sea-ice melting, changes in riverine inputs and sediment dynamics affected the benthic environment. Taxa analyzed for stable oxygen isotope composition of carbonates show the lowest δ^{18}O values during intervals within the MCA and the highest during the late LIA, which is consistent with a 1° to 2°C cooling of bottom waters. Faunal and isotopic changes during the cooler LIA (1300–1850 CE) are most apparent at ~1500–1850 CE and are particularly pronounced during 1850 to ~1900 CE, with a ~0.5 per mil increase in δ^{18}O values of carbonates from median values in the analyzed taxa. This very cold 50-year period suggests that enhanced summer sea ice suppressed productivity, which is indicated by low sediment biogenic silica values and lower δ^{13}C values in analyzed species. From 1900 CE to present, declines in calcareous faunal assemblages and changes in dominant species (*Cassidulina reniforme* and *P. pseudopunctillata*) are associated with less hospitable bottom waters, indicated by a peak in agglutinated foraminifera from 1950-1990 CE.

Keywords: benthic ostracodes, benthic foraminifera, stable isotopes, biogenic silica, paleoceanography, late Holocene, microfossils, Arctic Ocean

————————

INTRODUCTION

The recent acceleration of Arctic Ocean warming (Timmermans et al. 2018), freshwater storage (Proshutinsky et al. 2019), river discharge (Rawlins et al. 2010; Rood et al. 2017) and declines in sea ice extent, concentration and duration (Frey et al. 2015; Wood et al. 2015; Comiso et al. 2017) provide motivation to better understand past natural climate variability in the Arc-

tic. Proxy data from natural archives can provide a context for anthropogenically influenced climate change, and extend climate records back in time from the available instrumental observations (e.g. PAGES 2k Consortium, 2013). However, understanding the Arctic's response to Holocene climate change is difficult due to limited records with high spatial and temporal resolutions.

In this study, we infer paleoenvironmental signals from multiple proxy records at a continental shelf site in the Canadian Beaufort Sea over the past 2 millennia. The data were obtained using a set of composite cores collected from a mean water depth of 60 m – a jumbo piston core (JPC32), a gravity core (GGC30) and a multicore (MC29) – that were collected during a U.S. Coast Guard Cutter Healy 2013 (HLY1302) expedition (text-fig. 1). We constrain the timing of Medieval Climate Anomaly (MCA) and Little Ice Age (LIA) climatic fluctuations in this region using biogenic silica (opal), microfossil faunal assemblages and stable oxygen and carbon isotope ratios from a dominant ostracode species, *Paracyprideis pseudopunctillata,* and a benthic foraminiferal species, *Cassidulina teretis* s.l.

Oxygen isotopes ($\delta^{18}O$) of ostracode and foraminifera shell calcite can provide insights into benthic environmental change, including recording temperature variability and possibly sea ice change (such as increased salinity due to brine rejection from ice formation) or river water mixing to the seafloor. Water masses, and thus $\delta^{18}O$ values, in this region are affected not only by Pacific Water advected from the Bering and Chukchi Sea shelves but by localized processes, such as upwelling/downwelling, vertical mixing, sea ice freeze-up and melt-back, and Mackenzie River discharge. Since cryophilic ostracodes calcify and molt their shells during warmer months to an adult stage in order to reproduce (Horne, 1983; Athersuch et al. 1989), the $\delta^{18}O$ values of ostracodes reflect a summer water mass (Gemery et al. 2022). Carbon isotope variation (expressed as $\delta^{13}C$) reflects the composition of dissolved inorganic carbon (DIC) in seawater in which the shell calcified. In addition to specific bottom water microhabitats where the animal lives, $\delta^{13}C$ values may also be influenced by the organism's food sources and, like calcite $\delta^{18}O$, species-specific vital effects from shell calcification processes (stemming from the incorporation of metabolic CO_2 into the shell; Xia et al. 1997a,b; von Grafenstein et al. 1999; Wefer and Berger 1991; Rohling and Cooke 1999; Mackensen et al. 2000). Marine ostracodes are herbivores and detritivores (Smith and Horne 2002), feeding on particulate organic matter that reaches the sea floor and/or microbial components (Elofson 1941). $\delta^{13}C$ values at the sediment interface are affected by organic carbon flux rates to the sea floor (Buzas et al. 1993). Generally, higher productivity results in higher $\delta^{13}C$ values in the dissolved inorganic carbon that is incorporated into the shell. Lower (more negative) $\delta^{13}C$ values may indicate periods with less export of productivity to the seafloor and DIC from terrestrial carbon sources or microbial reworking. Reviews of stable oxygen and carbon isotopes in benthic ostracodes and foraminifera can be found in Holmes and Chivas (2002) and Ravelo and Hillaire-Marcel (2007).

Arctic climate variability during the last 2,000 years

Proxy records and models that examine the middle-late Holocene, north of 60°N, support a long cooling trend (i.e. the Neoglacial) beginning between 6 and 3 kyr ago, depending on the particular proxy examined, and extending until the late 20th century (Kaufman et al. 2009; Miller et al. 2010). The cooling during the late Holocene has been linked to the orbitally driven decrease in summer insolation, sulfates from volcanic eruptions, and the Maunder sunspot Minimum, 1650–1710 CE (Ammann et al. 2007). This declining temperature pattern is supported by a dataset of 59 Arctic/subarctic time-series multi-proxy records with annual-decadal resolution covering the last 2,000 years (PAGES 2k Consortium, 2013; McKay and Kaufman 2014; https://www.ncdc.noaa.gov/paleo-search/study/16973). The increase in sea ice extent during the late Holocene appears to be circum-Arctic, although there are different regional patterns of temperature and ice variability (e.g. de Vernal et al. 2005, 2013; Farmer et al. 2011; Bringué and Rochon 2012; Stranne et al. 2014; Stein et al. 2017; Hörner et al. 2016). Superimposed within the overall cooling trend are many multi-decadal to centennial-scale warmer or colder summer intervals that vary by region, as revealed in records from, for example, tree rings, Greenland ice cores, and lake sediments (Kaufman et al. 2009; PAGES 2k Consortium, 2013).

A period of milder climate identified in many records is the MCA, from ~800–1200 CE (e.g., Broecker 2001; Bradley et al. 2003b), but it is not synchronous in all regions (Bradley et al. 2003a,b; Kaufman et al. 2009; PAGES 2k Consortium, 2013). Proxy data are insufficient to determine if this was an Arctic-wide or wholly northern hemisphere event (Kaufman et al. 2009). Neoglacial summer cooling reached a maximum during the LIA (~1300–1850 CE; Miller et al. 2010). In many areas of the Arctic, glaciers and ice caps began to re-advance ~1300 CE (Anderson et al. 2008), with the coldest period between ~1550–1900 CE (Bradley et al. 2003a), ±50 years (Kaufman et al. 2009). Despite decreasing summer insolation through the 20th century, instrumental and proxy data show a "hockey-stick" shaped increase in temperature attributed to greenhouse gas emissions during the late 20th to early 21st centuries (Mann et al. 2008; Miller et al. 2010; IPCC, 2021). This warming is globally ubiquitous and amplified in the Arctic (e.g. McKay and Kaufman 2014; PAGES 2k Consortium, 2013 and references therein).

Environmental significance of microfossil species

Micropaleontological studies of benthic ostracodes and foraminifera have demonstrated that faunal biofacies record regional-scale and short-term ecosystem changes linked to sea-ice cover, surface productivity, and bottom temperature (e.g. Scott et al. 2009; Cronin et al. 2010; Poirier et al. 2012; Polyak et al. 2013; Gemery et al. 2017, 2021). These benthic faunal records are interpreted by comparison with modern species distributions and their affinities. This comparison allowed us to consider environmental changes in temperature, salinity, productivity, sea ice, sediment substrate, the strength of Pacific water inflows and river inputs, and storm events as possible conditions that can alter species abundance and distribution.

All taxa discussed here are typical representatives of Arctic-subarctic shallow-water continental shelf fauna (Cronin et al. 2021). Specifically, in order to identify changes in water mass characteristics of Arctic-Pacific water vs. Atlantic water vs. freshened water from river inputs, we relied on published preferences concerning a taxon's ecological/environment habitats, which are commonly associated with temperature and salinity. For purposes of this study, we distinguish three water mass categories and the foraminifera and ostracode taxa used as indicators of each water mass:
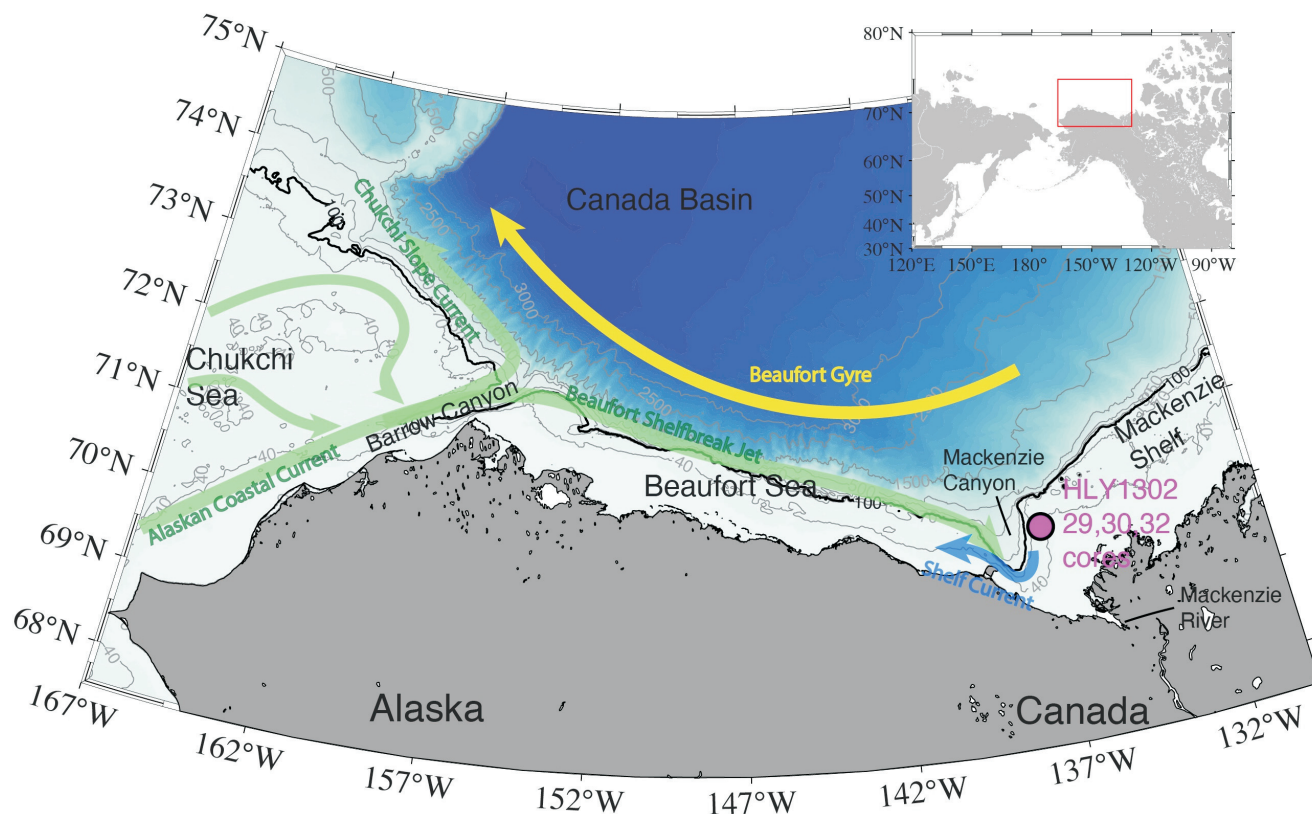
TEXT-FIGURE 1

Schematic circulation of Chukchi and Beaufort Seas and geographic names. The HLY1302 MC29, GGC30 and JPC32 (69.97°N, 137.24°W) core site (magenta circle) on the Mackenzie shelf in 60 m water depth. The green arrows denote the main pathway of Pacific-origin water exiting Chukchi Sea shelf and contributing to the Chukchi Slope Current to the west and Beaufort Shelfbreak Jet to the east. The blue arrow represents the Shelf Current in the vicinity of Mackenzie Canyon. The Beaufort Gyre (yellow arrow) situates in the Canada Basin. The bathymetry (in meters) is from The International Bathymetric Chart of the Arctic Ocean (IBCAO) v3 (Jakobsson et al. 2012).

1.) Indicators of Atlantic water are species commonly found in relatively warm water (>0°C) and high salinities (33–35), with wider depth tolerances (shelf and slope waters). Species indicating Atlantic water suggest considerably less influence of river inputs and sea ice melt. These species are: *Cassidulina teretis* s.l., *Cassidulina reniforme,* and *Semicytherura complanata* (see Supplementary Table 1 for a note on *C. teretis* s.l. taxonomy).

2.) Indicators of Arctic shelf water are versatile species more adapted to cold (=0-3°C) water and typically shelf salinity of 31-33. These species include *Islandiella helenae-norcrossi* (See Polyak et al. 2002, Supplementary taxonomic notes), *Elphidium excavatum forma clavatum, Sarsicytheridea bradii*, and *Kotoracythere arctoborealis.* The ecological affinities of *C. reniforme* also align with this group when it appears in an assemblage with *E. excavatum forma clavatum* (Hald et al. 1994).

3.) Low-salinity tolerant species are adapted to environments with high variability, with seasonal fluxes of salinity, food supply and temperature. Indicators of cold Arctic waters (=1°C) influenced by river inputs at polar surface water depths are *Paracyprideis pseudopunctillata* and two agglutinated species *Spiroplectammina biformis* and *S. earlandi.*

A more detailed ecological overview of the foraminifera and ostracode species in each water mass group is available in Sup-

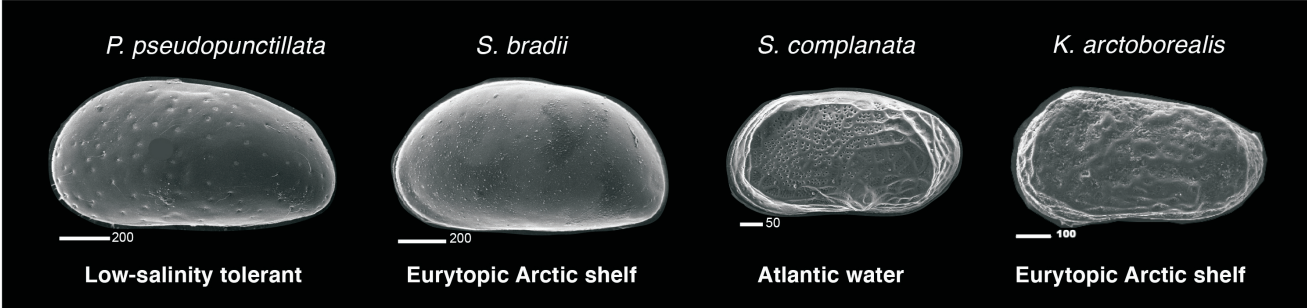plementary Table 1, with dominant ostracode species summarized in Table 1.

REGIONAL SETTING

Mackenzie Shelf Hydrography

The Mackenzie Shelf, a broad rectangular-shaped platform in the southeastern Beaufort Sea (text-fig. 1; width ~120 km; length ~530 km), is one of most estuarine of all the panarctic shelves (Macdonald et al. 1989). The Mackenzie River is the fourth largest of the Arctic rivers, discharging ~280 km^3 (±25) annually (Melling 2000) to the Mackenzie Shelf, mostly between May and September (Macdonald et al. 1998). During summer, this equates to a 3.7- to 10-meter-thick freshwater surface layer across the shelf (Macdonald et al. 1998; Carmack et al. 1989; Jackson et al. 2015) that is separated from the underlying cold saline water by a seasonal (summer) halocline (average salinity 20; Carmack et al. 1989).

Beaufort Sea shelf waters are mainly derived from relatively nutrient-rich Pacific Ocean waters advected from the Bering Strait and Chukchi Sea. Flowing northeastward closest to shore (~50-m isobath) is the Alaska Coastal Current (ACC) that mainly transports warm (T>3°C), low-salinity (S=30-32) and nutrient-poor Alaskan Coastal Water in summer (text-fig. 1; Weingartner et al. 2005; Nikolopoulos et al. 2009). Most of the

TABLE 1
Dominant ostracode species used in the HLY1302 composite cores (multicore [MC29], gravity core [GGC30], and piston core [JPC32]) to infer water mass changes at the Mackenzie shelf site. SEM photos taken from Gemery et al. 2015.

Species	typical temperature	typical salinity	typical water mass	sediment substrate	food preference	representative climate zone	primary modern distribution*	mode of life	primary ecological reference(s)
Paracyprideis pseudopunctillata	cold (≤1°C)	euryhaline, river proximal	winter water with fresher inputs	fine silty muds	phytodetritis	arctic-subarctic / circum-Arctic	Nearshore waters off Greenland, Norwegian, Kara, Laptev, East Siberian, Beaufort, Chukchi Seas, and Norton Sound in Bering Sea	infaunal	Stepanova, 2006
Sarsicytheridea bradii	eurythermic but more common in ≤4.5°C	normal marine (31-33)	Pacific-Arctic waters	sands and silts	phytodetritis	arctic-subarctic / circum-Arctic	North Atlantic (north of Cape Cod and Georges Bank), Ungava Bay, Frobisher Bay, Hudson Bay, Gulf of Maine, straits of the Canadian Arctic Archipelago, Newfoundland, Labrador Sea, waters off Great Britain, Ireland, Norway, Greenland, Franz Josef Land, Spitsbergen, Novaya Zemlya, White, Baltic, North, Barents, Kara, Laptev, East Siberian, Chukchi nearshore waters off Aleutian Islands, Anadyr Bay, Bering, Norton Sound, nearshore waters off Alaska	infaunal	Stepanova, 2006; Freiwald and Mostafawi, 1998; Hazel, 1970
Semicytherura complanta	cold (≤0-3°C)	normal marine, but high abundance in ≥33	winter water	sands and silts	unknown	arctic-subarctic / circum-Arctic	Areas where a polynya forms during wintertime; Greenland, White (southern inlet of the Barents Sea), Barents, Norwegian, Kara, Laptev, East Siberian, Chukchi, Bering, Beaufort Seas; Labrador Sea, Ungava, Frobisher, and Hudson bays, straits of the Canadian Arctic Archipelago, Ireland	infaunal	Stepanova, 2006; Brouwers et al., 2000; Cronin et al., 1994
Kotoracythere arctoborealis	cold (≤0-3°C)	euryhaline/ lower salinity areas incl. ~19 - 32	winter water also with fresher inputs	sands and silts	unknown	arctic-subarctic / Western Arctic	Protected waters in Chaunskaya Bay (Eastern Siberian, Sea Shelf, Bering Sea around St. Lawrence Island, Chukchi Sea north of the Bering Strait, NE Chukchi	unknown	Gemery et al., 2021; Cronin et al., 2021

Pacific-origin waters (including warm and fresh Pacific Summer Water and cold and salty Pacific Winter Water) from the other pathways in Chukchi Sea eventually rejoin to the ACC before draining off the shelf via Barrow Canyon (Lin et al. 2016, 2019b). The Barrow Canyon outflow then forms the Beaufort Shelfbreak Jet to the east. The Beaufort Shelfbreak Jet is surface-intensified in summer with significant seasonal variation (Nikolopoulos et al. 2009). It progresses eastward to the Canadian Beaufort Sea through the Mackenzie Canyon (Lin et al. 2020, 2021). Besides the Shelfbreak jet, the primary circulation on the Mackenzie Shelf, the Shelf Current, is predominantly wind-driven (Kulikov et al. 1998; Lin et al. 2020), and the anticyclonic Beaufort Gyre is dominant further offshore in the Canada Basin. Driven by wind, upwelling and downwelling commonly occur in both the Alaskan and Canadian Beaufort Sea, and play an important role in shelf-basin interactions (e.g., Foukal et al. 2019; Lin et al. 2019a; 2021). Upwelling commonly brings up warm and salty Atlantic water (T -1°C to 3°C and S 34-35) that generally resides at depth (below 150m on the slope and even deeper in the basin, Nikolopoulos et al. 2009), while downwelling can transport waters in the lower shelf layer into the basin (Lin et al. 2021). Mackenzie Shelf waters are modified by multiple factors, including vertical mixing, winds, ice and river runoff (text-fig. 1; Macdonald et al. 1987; Williams et al. 2008). Hence, water mass analyses on the Mackenzie Shelf are not necessarily straightforward (Carmack et al. 1989; Macdonald et al. 1989).

Sea surface temperature varies during summer (1°C to 10°C), but below ~40m, water temperatures remain ~< -1 to -2°C

year-round (Macdonald et al. 1987) and salinities are between 30.4 and 34.4 (Carmack et al. 1989), These general patterns are also consistent with recent bottom salinity and temperature measurements from conductivity-temperature-depth (CTD) profiling system collections (Okkonen 2013; as shown in text-fig. 2a,b). During fall and winter (November-April), winds, cooling and freezing flush out low-salinity surface water and break down the shelf stratification so the water column is vertically well-mixed and uniform in temperature and salinity (Macdonald et al. 1987). Sea ice covers the Mackenzie Shelf from September/October to May and can reach 2–3m thick (Melling and Riedel 1996). In the vicinity of our core site in winter, mean salinity is 32.15 (±0.05) and mean temperature is -1.76°C (±0.01°C; Jackson et al. 2015).

MATERIAL AND METHODS

Coring, sedimentology, sampling

The MC29, GGC30, JPC32 cores (69.97°N, -137.24°W, 60 m) were collected during expedition HLY1302 in summer 2013 onboard USCGC *Healy*. The site, in which all cores were collected, was located in the moat of a diapiric-like feature caused by methane gas hydrate decomposition during a prior warming period, which enabled recent, well-laminated sedimentation to occur. Additional description of the site is available elsewhere (Seidenstein et al. 2018). Cores were sub-sampled in September of 2016, 2018 and again in May 2019, including a second multicore, at Woods Hole Oceanographic Institution (WHOI). The sediment was primarily dark gray clay-mud. Altogether, core samples were taken every centimeter from MC29A and
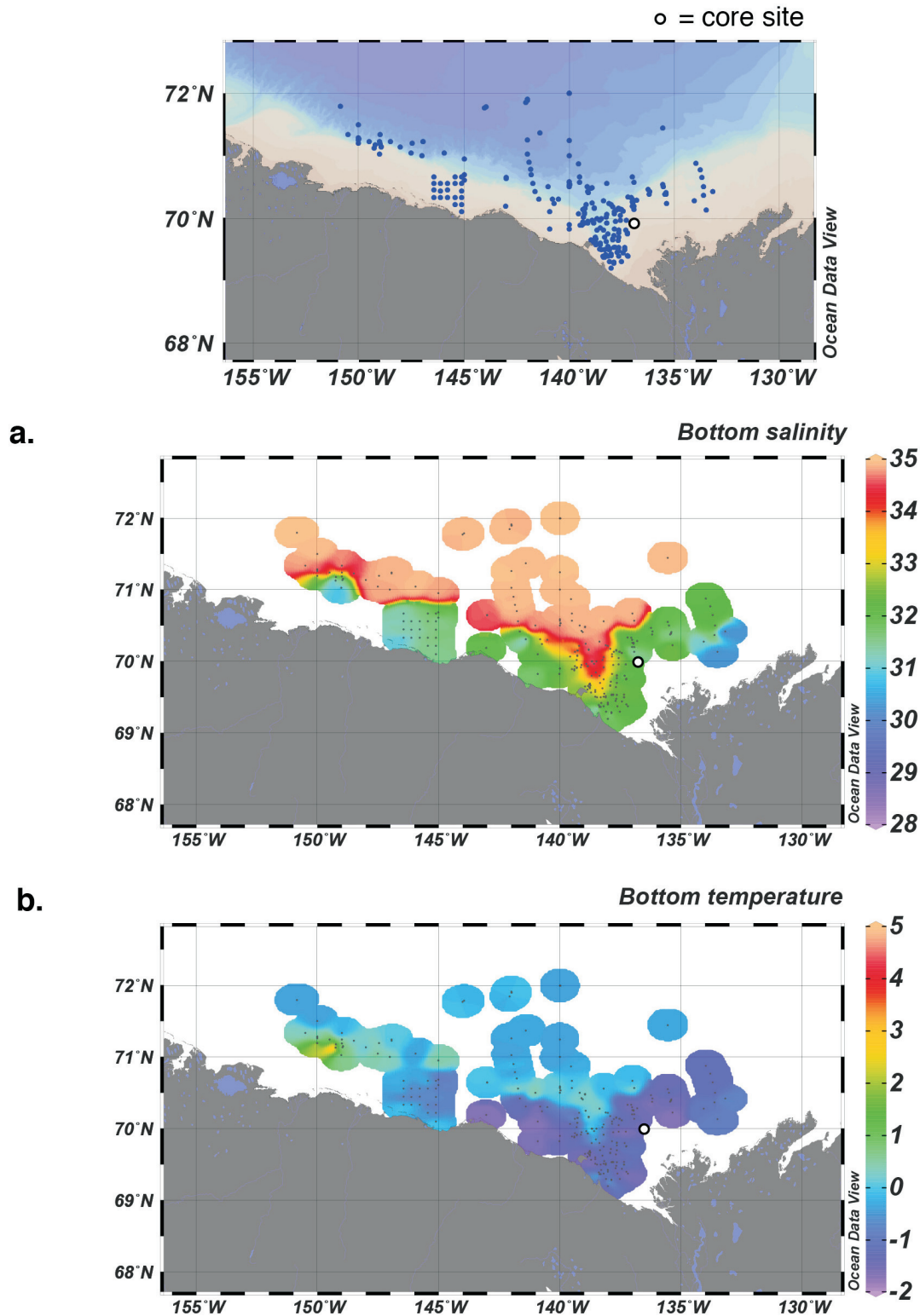
TEXT-FIGURE 2

Near-bottom summer a.) salinity and b.) temperature measurements (n=238) from a subset of CTD collections during August and September, 1990–2012 (Okkonen 2013), with the core site denoted by a white circle. Archived data sets from which the CTD summary data were derived (detailed in Grebmeier et al. 2015, Appendix G1) include: The Bering-Aleutian Salmon International Survey (BASIS), Chukchi Sea Offshore Monitoring in Drilling Area – Chemical and Benthos (COMIDA), R/V *Mirai*, University of Alaska Fairbanks Institute of Marine Science, Japan Oceanographic Data Center (JODC), NOAA's National Centers for Environmental Information (ww.ncei.noaa.gov), Russian-American Long-term Census of the Arctic (RUSALCA), Western Arctic Shelf-Basin Interactions project (SBI), Shell Oil, Study of the Northern Alaska Coastal System (SNACS)/ Bowhead Whale Feeding Ecology Study (BOWFEST), HLY1104, and Louis S. St. Laurent. Figure created using Ocean Data View software (Schlitzer 2018).

MC29B, and at 2-cm intervals from GGC30 and every 6cm from JPC32. Samples of 1-cm-thick slices at 1-cm intervals were taken from MC29A and MC29B, 2-cm^3 aliquots were taken every 2cm from GGC30 and 4-cm^3 aliquots were taken every 6cm from JPC32. Subsamples representing every 1cm increment of MC29B and each 10-cm interval in GGC30 and JPC32 were used for biogenic silica analysis. In addition, subsamples of MC29B in 2-cm intervals from 1 cm to 37 cm were assayed for the radioisotopes ^{210}Pb and ^{137}Cs in order to assess sedimentation rates and chronology in combination with the ^{14}C-dated intervals.

Microfossil sample processing and assemblage analysis

Sediments were washed through a 63-micron sieve and the residue oven-dried. Because the full round diameter of core MC29 was used, the average weight before processing was 30 g and the dry weight (after processing) of these 1-cm samples averaged 0.07 g. In GGC30 and JPC32, half of the core was sampled, and for each 2-cm interval, half of the half-round was taken. Sample weight before processing ranged from 30 to 44g and after processing averaged 0.03 g. Ostracodes were picked from all sediments greater than 125-micron size fraction to a microslide, sorted and identified using the taxonomy of Stepanova (2006) and Gemery et al. (2015). In accordance with counting protocols, up to 200 foraminiferal specimens were picked per sample (Seidenstein et al. 2018). All ostracode specimens found in the samples were picked and counted. Sample binning was done by combining count data from adjacent samples into one grouped sample comprising a larger depth interval; for ostracodes, samples from core MC29 was binned every 5cm, from core GGC30 every 10cm and from core JPC32 every 20cm (Supplementary Table 2; ostracode counts are expressed as number of valves; articulated carapaces were counted as two valves). For foraminifera data, individual samples contained sufficient specimen numbers (~200, with a few exceptions in core JPC32) and binning was not necessary. To identify significant changes in the faunal assemblages, 95% confidence limits were calculated using the algorithm for binomial probability from Raup (1991).

Stable isotope analyses

Stable oxygen and carbon isotope ratios were determined for calcium carbonate tests of *C. teretis* s.l. (n= 61) and *P. pseudopunctillata* (n=50; Supplementary Table 3). Data are reported in parts per thousand, or per mil (‰) deviations of the ^{18}O/^{16}O and ^{13}C/^{12}C ratios relative to the V-PDB (Vienna Peedee Belemnite) standard using laboratory standards calibrated against NBS19 and NBS18 (National Institute of Science and Technology). The ratios between ^{18}O/^{16}O and ^{13}C/^{12}C are expressed as delta values (δ^{18}O and δ^{13}C) as follows:

$$\delta^{18}O \text{ and } \delta^{13}C \text{ ‰} = [(R_{sample}/R_{standard})-1]*1000$$

where R = ^{18}O/^{16}O for δ^{18}O values or ^{13}C/^{12}C for δ^{13}C in the sample vs. the standard (Craig 1961; Coplen 1994). Values presented are not corrected for species vital effects, and are used as a relative measure for changes in water mass characteristics and/or meltwater/river inputs to the area.

Analyses of ostracode shell δ^{18}O and δ^{13}C values were conducted at the University of Maryland Center for Environmental Science in Solomons, Maryland, USA using a Thermo Fisher Scientific™ Delta V Plus stable isotope mass spectrometer coupled to a GasBench® peripheral preparation device. The preci-

sion of the measurements, based upon repeated measurements of carbonate standards, was determined to be ~ ± 0.1‰ for δ^{18}O and ~ ± 0.06‰ for δ^{13}C. Each isotope measurement consisted of two adult valves from the same sample interval that were cleaned of debris with water to achieve a weight of 40–90 ìg. Only adult ostracode specimens were used for geochemical analyses due to possible ontogenetic differences in shell chemistry during the life cycle. This also minimizes differences in shell weights due to varying shell size.

Foraminifera *C. teretis* s.l. δ^{18}O and δ^{13}C values were measured on an Elementar IsoPrime dual inlet mass spectrometer with a Multiprep peripheral at the National Environmental Isotope Facility at the British Geological Survey, Nottingham, UK. The precision of the data, based upon repeated measurements of the internal standard (Keyworth Carrara Marble calibrated against NBS), was determined to be ~ ± 0.04‰ for δ^{18}O and ~ ±0.03‰ for δ^{13}C. Each isotopic measurement comprised between 4-20 tests from the same sample interval. Tests from each sample were cleaned of debris with water to achieve a weight of 30–120 µg.

The intervals from which shells were derived depended on the abundance and preservation of specimens available in the sample. Because post-mortem processes can alter the original shell chemistry, only shells that were translucent or translucent-white were selected with no signs of early diagenetic effects.

Biogenic silica (opal)

Subsamples of HLY1302-MC29, -GGC30, and -JPC32 (n=79; Supplementary Table 4) were analyzed for biogenic silica (opal) at the USGS Biogenic Silica Lab in Menlo Park, CA, USA following the modified procedure of Mortlock and Froehlich (1989). This method is considered reliable for quantifying biogenic opal in opal-poor deposits. Briefly, samples were treated with 1N HCl overnight to remove carbonates and rinsed with distilled Nanopure water three times. Sediments were then freeze-dried, and 100 mg per sample was placed in a 0.1 M Na$_2$CO$_3$ solution at 85°C for four hours and cooled to room temperature overnight. 100 µL were reacted with a molybdate blue complex. Absorbances were measured at 812 nm wavelength using a Thermo Scientific GeneSys 10S spectrophotometer. Biogenic silica measurements were converted to opal concentrations using a 2.4 multiplication factor assuming 10% hydration (SiO$_2$ * 0.4 H$_2$O). To estimate error, we measured a subset of replicates; the average 1-sigma standard deviation for all replicates was 0.05 wt%. These assessments of precision and accuracy, in addition to comparisons of internal standards, suggest the estimate of error for the analysis is 0.06 wt%. Sample values are reported as a proportion of the sediment mass.

Chronology

Consecutive subsamples of MC29B in 2-cm intervals (0–38 cm) were analyzed on a low energy, high-purity germanium well detector for activities of ^{210}Pb and ^{137}Cs (Supplementary Table 5) at the St. Petersburg Coastal and Marine Science Center (SPCMSC), a United States Geological Survey lab in St. Petersburg, FL, USA. Each subsample (approximately 20-25g of wet sediment) was oven-dried at 60°C for 48 hours. The dried sediment was homogenized to a fine powder with a porcelain mortar and pestle. Dried ground sediments (6g) were sealed in polystyrene vials with epoxy to prevent gas emanation. The sample weight and counting container geometry were matched to a pre-determined calibration standard. The samples were sealed

a.

b.
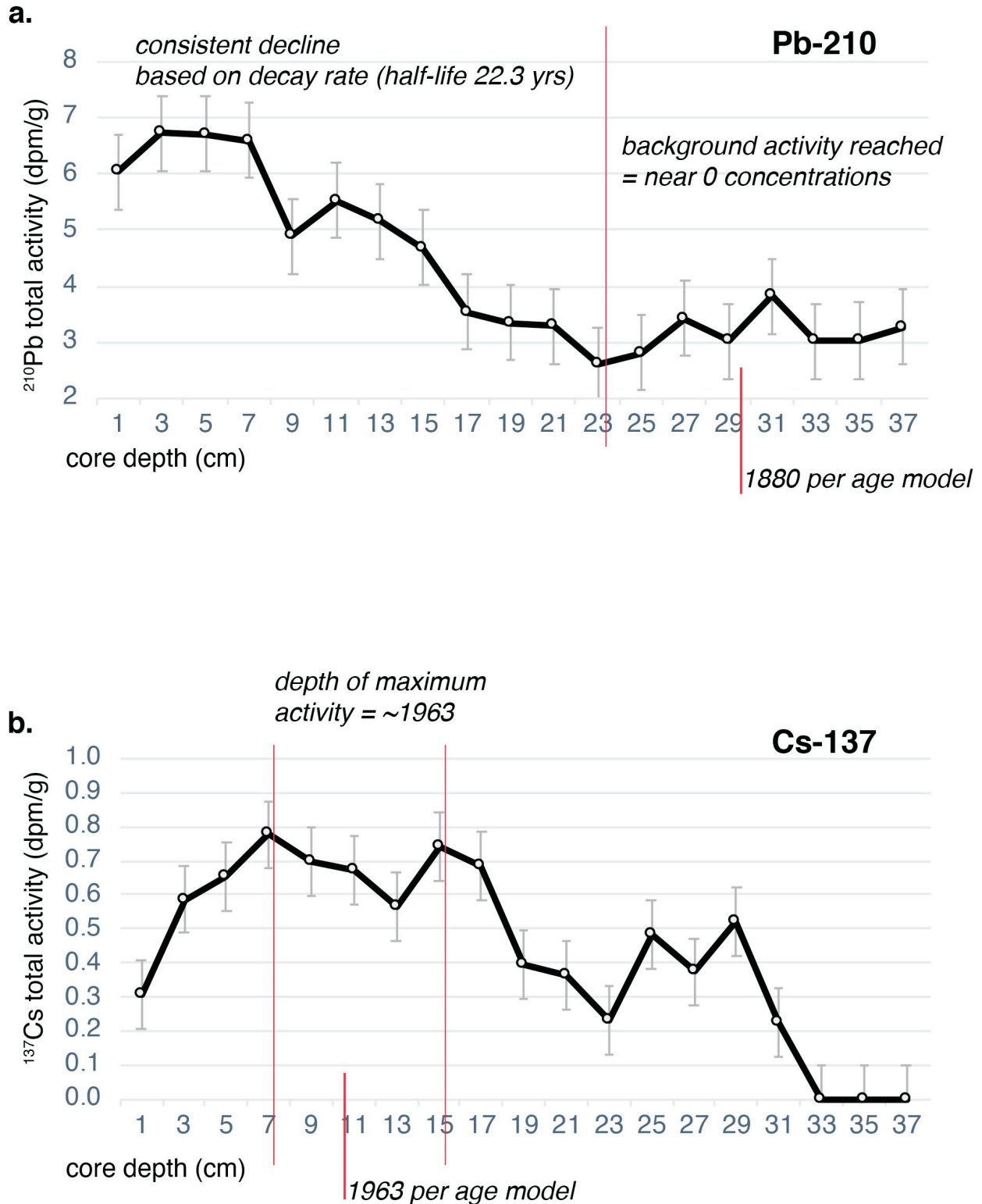
TEXT-FIGURE 3
Alignment of multicore 29 (MC29B) chronology with activities of ^{210}Pb and ^{137}Cs in the top 37cm of sediment. In MC29, the consistent decline of ^{210}Pb (measured in disintegrations per minute per gram [dpm/g]) shows baseline activity (indicated by the red bars) is reached at a 23- to 33-cm depth range. Based on the 22.3-year half-life decay rate of ^{210}Pb, near zero concentrations should be reached by the year 1880 and per our age model, this date coincides with ~29 cm depth. The temporal change of ^{137}Cs radioactivity in MC29 shows the 1963 nuclear weapons testing maximum between 7–15 cm (indicated by the red bars), which is the depth of peak ^{137}Cs maximum activity. Our age model for the core aligns with the 1963 date at ~11cm depth, which is the middle of the 7–15 cm ^{137}Cs maximum. The first testing of nuclear weapons in 1954 aligns with 13 cm, also within the range of peak ^{137}Cs activity.

TABLE 2
List of radiocarbon dates for the HLY1302 composite cores and calibrations using CALIB 8.2 software (Stuiver et al. 2021), the Marine20 calibration curve (Heaton et al. 2020) and a marine reservoir correction of ΔR =477±60 years (Pearce et al. 2017). Yellow highlight denotes seven new samples measured to improve the age model of Seidenstein et al (2018).

| | | | | | | | *BP* before present 1950 CE | | | |
| | | | | | | | Calibrated age range BP (2σ confidernce) | | | |
Accession #	Submitter Identification	Depth composite (cm)	Material	Uncalibrated age (yr BP)	Age eror (yr)	ΔR	from	to	2 sigma % confidence	median age (BP)
OS-106827	HLY1302 MC-29A	30	mixed benthics	615	20	no	0	223	95.4	80
OS-154540	HLY1302_GGC30_15-17cm	36	mollusc	1,090	15	477 ± 60	0	244	95.4	96
OS-154541	HLY1302_GGC30_45-47cm	66	mollusc	1,330	15	477 ± 60	130	483	95.4	318
OS-130828	HLY1302_GGC30_154-156cm	175	mollusc	1,760	15	477 ± 60	523	849	95.4	678
OS-154543	HLY1302_GGC30_172-174	195	mollusc	2,050	30	477 ± 60	772	1161	95.4	964
OS-154650	HLY1302_GGC30_175-177	196	mollusc	2,010	55	477 ± 60	709	1135	95.4	919
OS-154544	HLY1302_GGC30_235-237cm	256	mollusc	2,130	20	477 ± 60	878	1244	95.4	1047
OS-106830	HLY1302 GGC-30, bot corecatcher	311	mixed benthics	2,340	20	477 ± 60	1064	1426	95.4	1258
OS-130709	HLY13-02 JPC32, 70-72 cm	372	mollusc	2,530	20	477 ± 60	1278	1642	95.4	1452
OS-130710	HLY13-02 JPC32, 250-252 cm	552	mollusc	2,890	20	477 ± 60	1681	2095	95.4	1875
	Sediment reworked, not used:									
OS-131451	HLY13-02 JPC32, 260-262 cm	562	mixed benthics	3,180	20	477 ± 60	2010	2445	95.4	2232
OS-154603	HLY1302_JPC32_ 340-342cm	642	mollusc	2,980	15	477 ± 60	1765	2206	95.4	1986
OS-130711	HLY13-02 JPC32, 380-382 cm	689	mollusc	3,380	20	477 ± 60	2308	2703	95.4	2497
OS-130825	HLY13-02 JPC32, 450-452 cm	752	mollusc	3,250	15	477 ± 60	2104	2568	95.4	2327
OS-154604	HLY1302_JPC32_ 500-502cm	802	mollusc	3,110	20	477 ± 60	1940	2339	95.4	2153
OS-130826	HLY13-02 JPC32, 620-622 cm	922	mollusc	3,570	15	477 ± 60	2499	2917	95.4	2724
OS-130827	HLY13-02 JPC32, 710-712 cm	1012	mollusc	3,700	15	477 ± 60	2697	3077	95.4	2869

for a minimum of three weeks prior to analysis to allow ^{226}Ra to reach secular equilibrium with its daughter isotopes ^{214}Pb and ^{214}Bi. The sealed samples were then counted for 24–36 hours. Detector efficiency was determined with IAEA RGU-1 reference material. Radioactive activities were decay-corrected to the date of field collection. The accumulation of both ^{210}Pb and ^{137}Cs is assumed to be constant from direct deposition but likely with some import from the watershed (text-fig. 3).

Radiocarbon dates from molluscs and mixed benthic foraminifera were generated using the National Ocean Sciences Accelerator Mass Spectrometer (NOSAMS) facility at Wood Hole, MA, USA. Ages were calibrated to calendar years BP with the Marine20 radiocarbon age calibration curve (Heaton et al. 2020) using the Calib version 8.2 software (Stuiver et al. 2021; text-fig. 4; Table 2). Because old Pacific waters are a component of the Beaufort Sea, we corrected for a regional reservoir age of 477±60 years based on late Holocene sediments absolutely dated by 3.6 ka Aniakchak volcanic ash (Pearce et al. 2017). Radiocarbon ages are reported using the BP 1950-time ^{14}C scale, meaning years before 1950 and also converted to calendar years (CE). The age model for MC29 was fit linearly using the regression equation based on the most recent radiocarbon date at 30cm and back-dated under the assumption that the 0–1cm interval represents the year the core was collected (text-fig. 4; calendar year 2013, -63 years BP). The activity levels of ^{137}Cs and ^{210}Pb in MC29 were used to corroborate the MC29 age model from the radiocarbon dates. By matching the foraminiferal faunal assemblages of GGC30 with MC29, it was determined by Seidenstein et al. (2018) that 20 cm was missing from the top of GGC30. Likewise, we followed that study's determination that 301 cm was missing from the top of JPC32 to align with the bottom of GGC30. Although there is some uncertainty when splicing the two cores chronologically,

two sequential radiocarbon dates from JPC32 support this assumption. Linear sedimentation rates were calculated by dividing the difference in depth by the difference in age between two samples. These rates do not account for possible compaction of sediment with depth, elastic rebound of sediment cores with decreased pressure, or coring disturbance.

Statistical analyses

Multivariate statistical analyses were carried out using the Paleontological Statistics (PAST) software package, version 3.24 (Hammer et al. 2001). We calculated relative frequencies (percent abundance of total assemblage) for each species and used this relative abundance data in the correspondene analyses. Principal component analyses (PCA) were used to group ostracode and foraminifera species by their similarities/differences in dominance based on samples designated by year groups (text-fig. 5a,b).

RESULTS

Correlation of radioisotopes and AMS ^{14}C dating

In MC29, a consistent logarithmic decline of ^{210}Pb shows that background activity (~3 dpm/g) was reached at the 23-cm core depth (text-fig. 3a). Based on the 22.3-year half-life decay rate of ^{210}Pb, near zero above background activities should be reached by the year 1880 CE. Per our age model, the 1880 CE date coincides with ~28 cm depth. There are a few minor spikes of slightly higher ^{210}Pb activity sediment (~1dpm/g) after 23 cm that may be a consequence of sediment transport.

The temporal change of ^{137}Cs radioactivity in MC29 shows the 1963 nuclear weapons testing maximum between 7–15 cm, which is the depth of peak ^{137}Cs activity (text-fig. 3b). Our age model aligns with the 1963 date at 11cm depth, which is the

a. Calibrated age ranges and *(Marine20 median calibrated age in calendar yrs CE and BCE)*
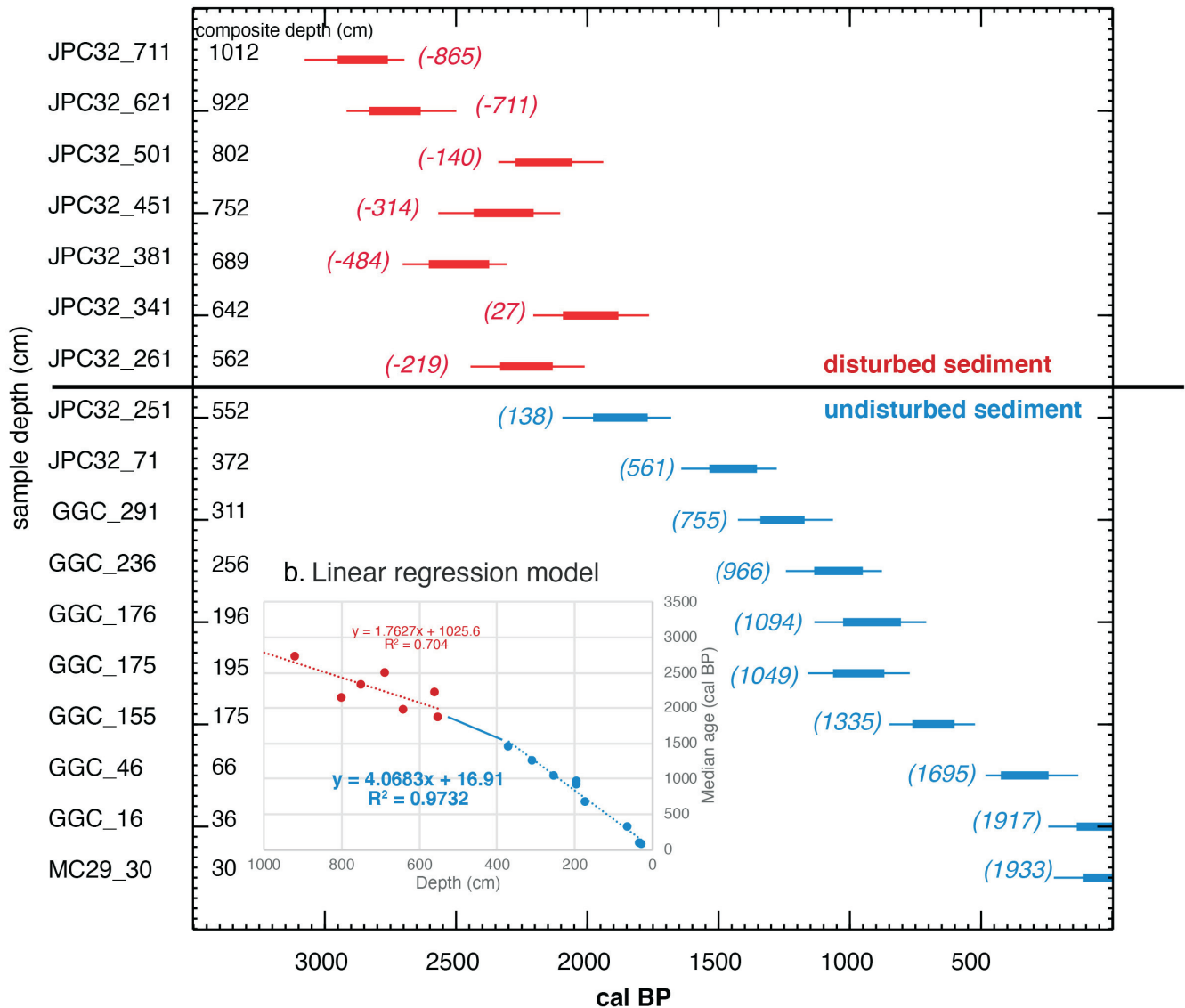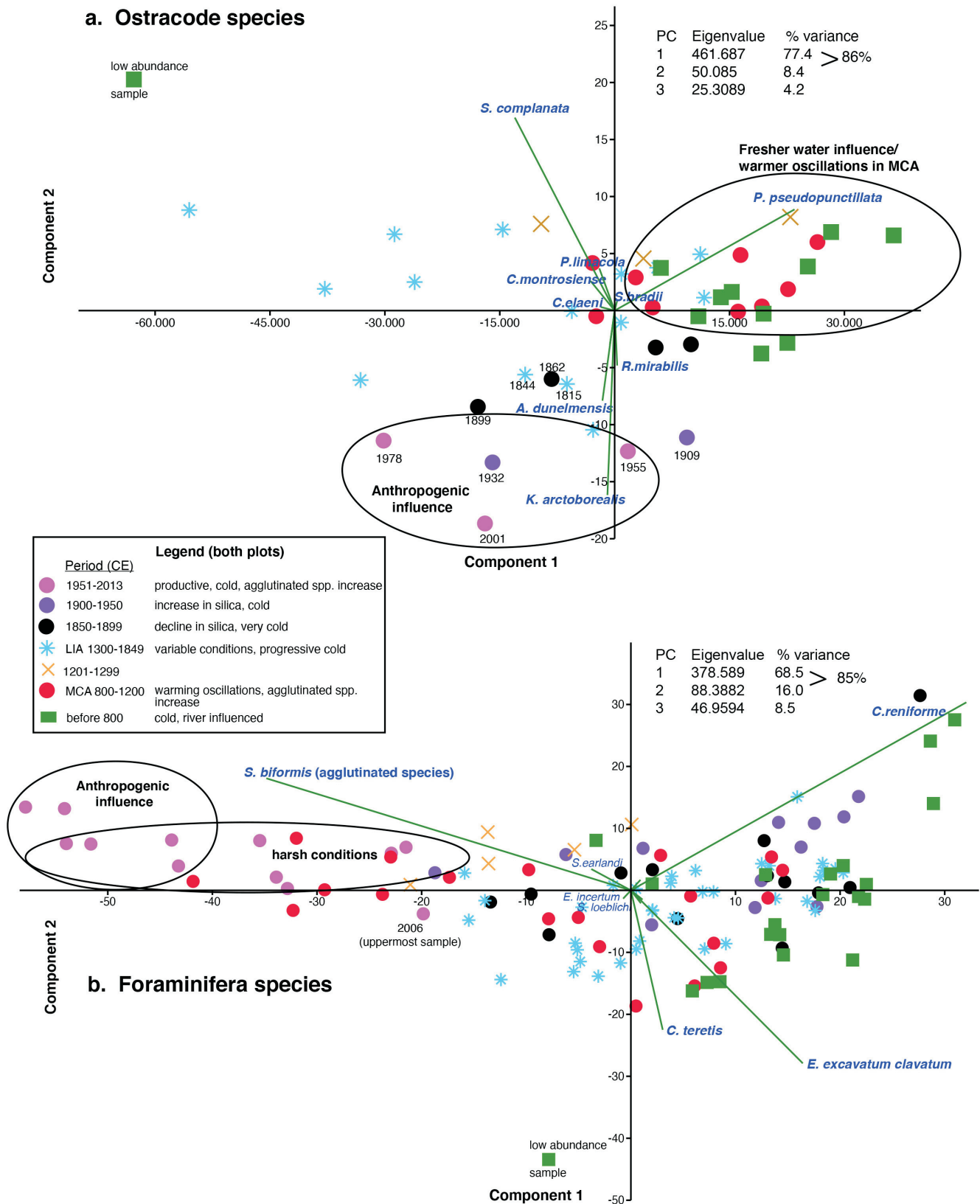
TEXT-FIGURE 4
a. Age-depth model of HLY1302 composite cores, MC29, GGC30, JPC32. Seventeen median radiocarbon dates shown with 2-sigma error bars (~95% of the measurements fall within the bar range) in years before present (BP) and calendar years (in red parentheses). b. the regression model (y= 4.0683x + 16.91) is used to linearly tie the 10 most recent dates of the undisturbed sequence.

middle of the 7–15 cm ^{137}Cs maximum. The first testing of nuclear weapons in 1954 aligns with 13 cm, within the beginning range of peak ^{137}Cs activity. Overall, both curves support that sedimentation dominates over bioturbation at the core site (text-fig. 3). Both curves corroborate the dates used in the MC29 section of the age model.

Seventeen radiocarbon dates show that before ~550 cm composite depth, the sediments of JPC32 are disturbed (Table 2; text-fig.4a). A regression model with an r^2 =0.97 is used to linearly tie the 10 most recent dates of the undisturbed sequence (text-fig. 4b). Therefore, the record we present begins at 0CE

(2ka BP), or 490cm composite depth, and ends in the year 2013 at the top of MC29. We have confidence that the sedimentation was relatively undisturbed through this period based on sequential radiocarbon dates and ^{137}Cs and ^{210}Pb activity. Sedimentation rates ranged from 22cm (in MC29) to 24cm/century (in GGC30 and JPC32). This sedimentation rate in MC29 is also supported by the ^{210}Pb activities (Supplementary Table 5).

The age uncertainty associated with the radiocarbon dates precludes the study of decadal-scale variability, but the faunal and isotopic fluctuations enable the evaluation of sub-centennial environmental changes and comparison with modern conditions.

a. Ostracode species

PC   Eigenvalue   % variance
1   461.687   77.4 ⎫ 86%
2   50.085   8.4   ⎬
3   25.3089   4.2   ⎭

low abundance sample

Fresher water influence/ warmer oscillations in MCA

S. complanata

P. pseudopunctillata

P. linicola
C.montrosiense
C.elaeni
S.bradii

R.mirabilis

1862
1844
1815
A. dunelmensis
1899

1978
1932
1955
1909

Anthropogenic influence

K. arctoborealis

2001

Component 1

Component 2

Legend (both plots)

Period (CE)

● 1951-2013	productive, cold, agglutinated spp. increase
● 1900-1950	increase in silica, cold
● 1850-1899	decline in silica, very cold
✳ LIA 1300-1849	variable conditions, progressive cold
✕ 1201-1299	
● MCA 800-1200	warming oscillations, agglutinated spp. increase
■ before 800	cold, river influenced

b. Foraminifera species

PC   Eigenvalue   % variance
1   378.589   68.5 ⎫ 85%
2   88.3882   16.0 ⎬
3   46.9594   8.5   ⎭

C.reniforme

Anthropogenic influence

S. biformis (agglutinated species)

harsh conditions

S.earlandi

E. incertum
S. loeblich

2006
(uppermost sample)

Component 2

C. teretis

E. excavatum clavatum

low abundance sample

Component 1

TEXT-FIGURE 5
Principal component analyses of (a.) ostracode assemblages and (b) foraminifera assemblages colored by major time periods.
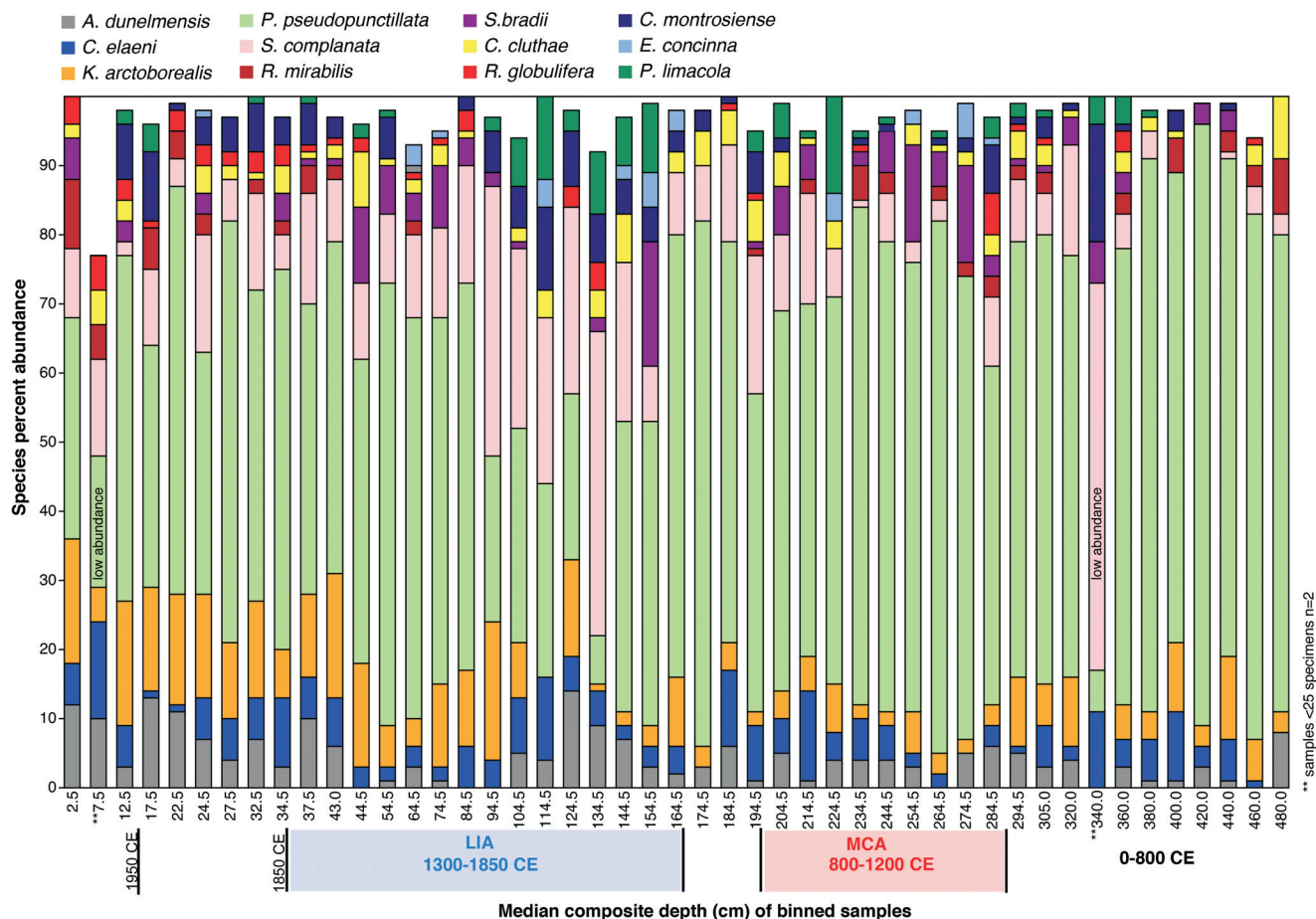
TEXT-FIGURE 6
Stack plot of ostracode species that make up 98% of the assemblages by composite depth.

Ostracode and foraminifera faunal assemblages

A total of 11 benthic ostracode species were identified (Supplementary Table 2), and are listed in order of percent abundance within the 2 kyr record (n=4356 specimens in 52 binned samples; text-fig. 6): *Paracyprideis pseudopunctillata* (55%), *Semicytherura complanata* (12%), *Kotoracythere arctoborealis* (8%), *Cytheropteron elaeni* (5%), *Acanthocythereis dunelmensis* (4%), *Cytheropteron montrosiense* (3%), *Sarsicytheridea bradii* (3%), *Cluthia cluthae* (3%), *Rabilimis mirabilis* (2%), *Palmenella limicola* (2%), *Roundstonia globulifera* (1%). These species make up 98% of the assemblage composition during the 2 kyr record. The number of specimens per binned sample ranged from 18 to 274, with an average of 84 specimens (± 50) per grouped sample. Two of the binned samples contained less than 25 ostracode specimens (text-fig. 6; Supplementary Table 2). Of the benthic foraminiferal fauna identified by Seidenstein et al. (2018), 90% of the assemblage during the last 2 kyr was comprised by varying proportions of calcareous species *Cassidulina reniforme* (32%), *Elphidium excavatum forma clavatum* (19%), *Cassidulina teretis* s.l. (11%), *Stainforthia feylingi* (7%), *Buccella frigida* (3%), *Stainforthia loeblichi* (3%), *Elphidium incertum* (2%), and agglutinated species *Spiroplectammina biformis* (12%), and *Spiroplectammina earlandi* ([1%]; n=24,767 total specimens in 121 binned samples; selected species, text-fig. 7). Upon further investigation of

the foraminifer fauna, we believe *Islandiella helenae-norcrossi* may be a component of specimens identified as *C. teretis* s.l.

The last 2,000 years were subdivided into four major time periods based on climate oscillations identified by other published proxy compilations (e.g. Kaufman et al. 2009; PAGES 2k Arctic, 2013; McKay and Kaufman 2014) and fluctuations of dominant foraminifera and ostracodes species abundance and isotope values (text-fig. 8). The lowermost zone 1, from 300-490 cm, covers 0-800 CE. Zone 2, 190-300cm, covers the MCA (800-1200 CE). Zone 3, 35-170 cm, covers the LIA (1300-1850 CE). The uppermost Zone 4, 0-35 cm covers 1850 to 2013 CE. PCA analyses (text-fig. 5a,b) show ostracode and, to a lesser degree, foraminifera species assemblage composition aligns with these periods, which are described below.

Zone 1 (0–800 years CE)

This period is characterized by the ostracode *P. pseudopunctillata* dominating >60–90% of the assemblages. *Kotoracythere arctoborealis* is a consistent species in the assemblage, and its abundances fluctuate from 0–12% in samples. *Sarsicytheridea bradii* and *S. complanata* are present in only some samples at very low percentages (<5%). Of the foraminifera, *C. reniforme* averages 43%, *E. clavatum* averages 24% (with a standard deviation of ± 8%, not shown, please refer to

TABLE 3
Summary of δ^{18}O and δ^{13}C isotopic data.

	δ^{18}O (‰ VPDB)		δ^{13}C (‰ VPDB)	
	P.pseudo	**C. teretis**	**P.pseudo**	**C. teretis**
Avg over 2ka record	3.8	2.3	-1.7	-1.2
stdev	0.31	0.18	0.48	0.32
n=	50	61	50	61
Avg last 100 yr	4.0	2.4	-1.6	-1.2
stdev	0.17	0.16	0.48	0.32
n=	6	16	6	16
Avg during end of LIA (1800-1900 CE)	4.1	2.3	-1.8	-1.2
n=	8	8	8	8
Avg during MCA	3.6	2.1	-1.8	-1.3
n=	9	10	9	10
‰ increase in δ^{18}O from MCA to LIA	0.5	0.2		
°C temperature decrease from MCA to LIA	~2	~1		
r² trend of increasing δ^{18}O from MCA to present (800-2013 CE)	0.26	0.38		
r² trend of increasing δ^{13}C over 2ka record			0.02	0.27

Seidenstein et al. 2018) and *C. teretis* s.l. (including possible *Islandiella*) averages 16% (standard deviation of ± 9%, text-fig. 5c) during this period. There is an interval of very low microfossil abundance from 330–350 cm (~640-670 CE) with 18 ostracode specimens denoted by a yellow highlight (text-fig. 5a) and 24–49 foraminifera specimens (2 samples). While it appears that several faunas rapidly changed in relative abundance within this interval, this should be considered an artifact due to low microfossil abundance.

Zone 2 (MCA, 800–1200 CE)

A notable change in the record during the MCA is signaled by distinct increases in the agglutinated species *S. biformis* to between 20% to 42% of the overall assemblage in 12 sample intervals within the depth range of 175-300cm, and this results in a decrease in *C. reniforme* to a proportion of between 5-25%. A near absence of *S. biformis* coincides with a short-term maxima of *C. teretis* at ~260-cm depth (~900 CE*). Paracyprideis pseudopunctillata* remains the dominant ostracode species (50-80% of assemblages), with some variable increases of *S. bradii* (5-15%) and the consistent presence of *K. arctoborealis* at low proportions.

Zone 3 (LIA, 1300–1850 CE)

The beginning of the LIA at ~1300 CE is marked by a precipitous decline in *P. pseudopunctillata* to between 6-30% of the assemblage. *Semicytherura complanata* reaches its highest abundances (44%) of the record during 1400 to ~1600 CE and *C. reniforme* declines from 45% to <20%. *Cassidulina teretis* (including possible *Islandiella*) increases modestly from ~4% to 26% with some variability, as does *K. arctoborealis*, which reaches 20% of the assemblage population at ~1600 CE. After 1600 CE, both *P. pseudopunctillata* and *C. reniforme* increase and remain the dominant species to 1850 CE.

Zone 4 (1850–2013 CE)

The most recent part of the record was sampled at consecutive one-centimeter resolution for benthic microfossils and represents a time-averaged faunal record of every 23 years from 1850 to 2013 CE. From 1850 to 1900 CE, dominant fauna *P.*

pseudopunctillata and *C. reniforme* decline in a somewhat stair-stepped manner from abundance highs of 60% to an average of 35% and 30% by the 1950s. While these species decline (after ~1950), agglutinated foraminifera *S. biformis* and *S. earlandi* sharply increase to abundances of 30–62% and 4–14%, respectively, and reach peak abundances ~1970 to 1990 (5–10 cm depth). Among the ostracode fauna, *P. pseudopunctillata* represents 19% of the assemblage ~1980 and 32% ~2000, with other taxa in the *Cytheropteron* spp. group (including *C. elaeni, C. inflatum, C. paralatissimum*) representing up to 38% of the assemblage. *Kotoracythere arctoborealis* maintains an average population of 13% during the entire zone and 18% in the uppermost interval. The most recent 20 years of the record shows the agglutinated species declining with a wider diversity of foraminifera representing the assemblage, notably, *C. reniforme* (12%) and *E. clavatum* (9%) co-dominate with *S. biformis* (17%). Other foraminifera that have significant increases in abundance since ~2000 CE include *Elphidium incertum* (12%) and *Elphidium bartletti* (8%), both of which prefer riverine-influenced habitats with sandy, shallow seafloor areas off estuaries (Polyak et al. 2002).

Biogenic silica (opal)

Biogenic silica is used as an indicator of marine primary production in the surface water from primarily diatoms, which are the dominant photosynthesizing marine organisms (Okazaki et al. 2005; Addison et al. 2013). The biogenic silica rain rate and subsequent burial in the sediments may suggest increased/decreased primary productivity resulting from a reduced/enhanced sea ice cover. Low percentages of biogenic silica content are generally found in glacial periods with more stable sea ice cover (Stein and Fahl 2000) and when there was no transport of Pacific surface waters through the Bering Strait. At our core site, biogenic silica concentration (n=79) averaged 1.2% ± 0.23, with maxima (outside of the standard deviation ranges) corresponding to a few intervals in Zone 1 between 100 and 400 CE and in Zone 4 from 1925-2013 (text-fig. 9a). Minima corresponded to intervals within Zone 2 during the MCA from 800–1150 CE, Zone 3 during the early LIA, and Zone 4 from 1850 to 1900.

Ostracode and foraminifera δ^{18}O and δ^{13}C

The δ^{18}O values of cryophilic ostracodes reflect summer water masses, since it is during the warmer months that ostracodes calcify their shells to an adult stage in order to reproduce (Horne 1983). More variability in temperature and salinity would be expected in summer than winter due to warmer temperatures, Mackenzie River discharge, and sea ice melt.

The δ^{18}O of *P. pseudopunctillata* (n=50) varied from +3.0 to +4.5‰, with an average value of +3.8‰ (± 0.31), and a core-top value of +4.2‰ (Table 3; text-fig. 9b). Ten replicate ostracode samples were measured from different sample intervals, and the average standard deviation of the δ^{18}O intra-sample measurements was 0.1‰ and for δ^{13}C, 0.4‰. Comparing δ^{18}O of this species in the Beaufort Sea to values from modern specimens in the northern Bering and Chukchi Sea shelves (at 75–80°N), we find average values to be lower in the Beaufort Sea by 0.6‰ (+4.4‰ [± 0.4] per Gemery et al. 2022). This suggests that δ^{18}O of bottom water on the Canadian Beaufort shelf may be lower overall due to some Mackenzie River water mixing to the 60 m seafloor. It is likely not due to temperature differences because values would be higher, and bottom temperatures have remained cold (<0°C). The δ^{18}O of *C. teretis*
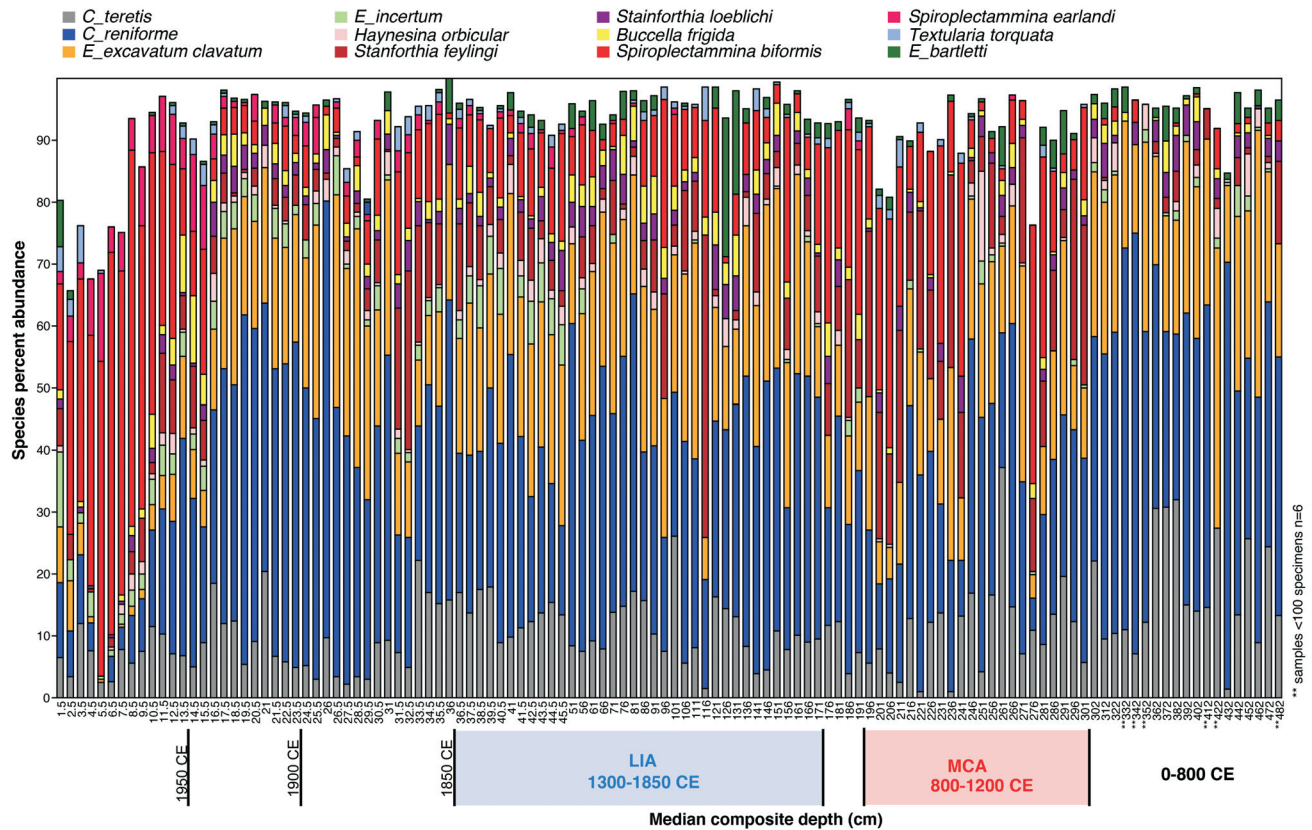
TEXT-FIGURE 7
Stack plot of primary foraminifera species that make up ~95% of the assemblages by composite depth. The *C. teretis* group might include members of the genus *Islandiella* requiring further studies.

s.l. (n=61) varied from +1.9 to +2.9‰, with an average value of +2.3‰ (± 0.18), and a core-top value of +2.6‰ (Table 3; text-fig. 9b).

The mean $\delta^{18}O$ values of both species from the MCA to post-LIA reveal a trend toward higher isotope values that, assuming temperature is the primary control, correspond to a 1-2°C decrease in bottom water temperature. The $\delta^{18}O$ values of *P. pseudopunctillata* ranged from +3.0‰ to +4.1‰ during the MCA and from 3.7‰ to 4.5‰ during the LIA. The $\delta^{18}O$ value for *C. teretis* s.l. varied from +2.0‰ to +2.3‰ during the MCA and from +2.3‰ to +2.6‰ during 1800-1900. Likewise, for the two species, mean $\delta^{18}O$ values during the last ~100 years (1900–2013) is higher than average values over the past 2 kyr (Table 3; text-fig. 9b).

The $\delta^{13}C$ values of *P. pseudopunctillata* fluctuated from –2.6 to –0.7‰, with an average value of -1.7‰ (± 0.48), and a core-top value of –2.4‰ (Table 3; text-fig. 9c). The $\delta^{13}C$ values of *C. teretis* s.l. varied from -2.0 to -0.6‰, with an average value of –1.2‰ (± 0.32), and a core-top value of –0.8‰ (Table 3; text-fig. 9c). A comparison of $\delta^{13}C$ values during the MCA and late- to post-LIA showed no significant change.

DISCUSSION

The ostracode, foraminifera, stable isotope, and biogenic silica records together demonstrate that bottom water conditions varied considerably during the past 2 kyr. Alongside species' fau-

nal changes (text-fig. 8) intervals with lower and higher $\delta^{18}O$ (text-fig. 9b) and $\delta^{13}C$ carbonate values (text-fig. 9c) can be used to identify periods of changing water masses. Here, we discuss how the fluctuations in proxy records (text-figs. 8 and 9) may reflect the presence of specific water mass and paleo-environmental conditions during and within the four chronological zones established above.

Cold Arctic bottom water during Zone 1 (0–800 years CE)

Dominant ostracode and foraminifera species support that cold, river-influenced Arctic shelf water was primarily present on the bottom during this period. This is evident by high abundances (>70%) of *P. pseudopunctillata* and a consistent presence (5–10%) of *K. arctoborealis* and foraminifera (24%) *E. clavatum*. Likewise, the abundance of *C. reniforme* alternates from 30 to 70% of the assemblage. However, the varying presence of *C. teretis* s.l. (possibly including *Islandiella*) (>10%) implies there may some sustained Atlantic water incursions onto the shelf (Jennings and Helgadottir 1994), especially during 370–570 CE when *C. teretis* s.l. and *C. reniforme* (Hald et al. 1994) combined comprise upwards of 60% of the assemblage. The Atlantic Water hypothesis must be tested with additional sediment cores and ecological studies of *Cassidulina* and *Islandiella*.

Stable isotope measurements of both species are not highly resolved during this period but do not fluctuate much from average values. The interval of low microfossil abundance (~600

CE), which is not resolved in this record, could be attributed to several possible scenarios, such as transport or dilution of the fauna from a storm event, or dissolution from diagenetic processes.

Variable warming, fluctuating conditions with Atlantic water incursions during Zone 2 (MCA, 800–1200 CE)

High abundances (>60% assemblage average) of *P. pseudopunctillata* continue during the MCA in addition to low and steady percentages of *S. complanata* and *K. arctoborealis*. Abundance of thermally adaptable *S. bradii* increases (~15% of assemblage) at ~870-1000 CE and 1100-1200 CE. The ostracode PCA (text-fig. 5a) identifies the MCA and the period before 800 CE as zones in which low-salinity tolerant *P. pseudopunctillata* is most dominant.

Atlantic water upwelling is evident from the fluctuating abundance of *C. teretis* s.l. The foraminifera PCA (text-fig. 5b) shows most samples in the MCA include more *C. teretis* s.l. and agglutinated species than the typical polar shelf species *C. reniforme*. Intervals in the early, mid-, and late part of the MCA also see short but significant increases of agglutinated foraminifera *S. biformis* from near zero to 32-42% abundance. Generally, an increased frequency of agglutinated taxa has been attributed to harsher or less stable environmental conditions, such as turbidity, irregular food, acidity, or anoxia (Schröder-Adams et al. 1990; Jennings and Helgadottir 1994; Korsun and Hald 2000; Perner et al. 2012, 2015). Measurements of biogenic silica during the early and late MCA are the lowest sustained percentages of the record, suggesting extended periods of somewhat depressed productivity. There also is a strong negative excursion of binned δ^{13}C of *P. pseudopunctillata* and lower δ^{13}C values of *C. teretis* s.l. that corroborate reduced productivity.

Stable oxygen isotopes of *P. pseudopunctillata* are the lightest of the record (δ^{18}O = 3.0-3.3‰) and suggestive of less saline or warmer bottom waters, yet the δ^{18}O values of *C. teretis* s.l. show only limited changes from average values. These patterns could result from the fact that ostracodes most commonly reach adulthood in summer (Horne 1983), so the δ^{18}O of *P. pseudopunctillata* is reflective of summer bottom temperatures (Gemery et al. 2022) whereas the foraminifera signal integrates more of the whole year. If the lower δ^{18}O oscillations reflect bottom water warming, this may have resulted from warmer summer fluctuations or possibly changes in the extent, strength or temperature of Atlantic Water affecting the core site. Further, we conclude that the lower δ^{18}O values reflect a temperature shift because freshwater changes due to variation in the Mackenzie River outflow are not thought to be significant during the MCA (Wickert 2016). Overall, variable warming during this period is corroborated by a reduction in sulfate aerosols from explosive volcanism (Crowley 2000; Goosse et al. 2005) and high levels of total solar irradiance (Bradley et al. 2003a,b; Beer 2000). It may also be related to circulation anomalies in the northern hemisphere, possibly involving a shift in the mode of the North Atlantic or Arctic Oscillation (Bradley et al. 2003a,b).

Cooling and episodic sediment disturbance during Zone 3 (LIA, 1300–1850 CE)

After 1300 CE, the abundance of *P. pseudopunctillata* declines, and from 1400 to 1600 CE, *P. pseudopunctillata* reaches its lowest presence (10–30%) of the record, which is possibly due to a sediment grain size change. Furthermore, *Semicytherura complanata* and *K. arctoborealis,* which are found in coarser

sediments (Gemery et al. 2022), increase during this 300-year period, as well as low proportions (8–24%) of agglutinated foraminifera *S. biformis*. Sediments on the Beaufort Sea shelf are generally high in silt and clay, with minimal to no sand (Scott et al. 2008). The ecological tolerances of *P. pseudopunctillata* could accommodate slight changes in temperature or salinity that would be feasible during this period and would be unlikely to affect its abundance. Also, δ^{18}O values do not suggest higher salinity or extreme temperature change. We surmise that it was stronger bottom water currents that winnowed the very fine silts to create a coarse sediment bottom texture unfavorable to *P. pseudopunctillata* (Gemery et al. 2022).

Atlantic water upwelling is evident from the abundance of *C. teretis* s.l. (4–26%) and *C. reniforme* (17–48%) during the early and mid-LIA. After 1600 CE, the rebound of *P. pseudopunctillata* to 45–65% abundance, the steady increase in *C. reniforme* to 46–52% and continuous presence of *E. clavatum* (ranging from 13 to 35%) and *S. biformis* (ranging from 1 to 17%) all support a scenario where bottom water was generally influenced by very cold-water masses as the LIA progressed. Cold water masses are indicated by the δ^{18}O values of *P. pseudopunctillata*, recording three high values >4.0‰ before 1750 CE. At 1750 CE, there is one δ^{18}O measurement of 3.3‰, just below average values, but then values increase to above or within average standard deviation ranges. δ^{18}O values of *C. teretis* s.l. remain relatively constant within one standard deviation of variation through the LIA. Our proxy results support a cooling trend from the MCA to LIA documented, which is demonstrated in the mean-annual temperature reconstructions from the GISP2 ice core (Alley et al. 1999) and terrestrial records of arctic summer temperatures (Kaufman et al. 2009). The mean δ^{18}O values of both species from the MCA to post-LIA shows a trend toward higher values that corresponds to a 1–2°C decrease in bottom water temperature. Productivity, as reflected in biogenic silica measurements, varied from 1300–1500 CE but thereafter remained high during most of the period until 1850 CE.

Continued near-freezing conditions and shifts in organic carbon and seafloor environment during Zone 4 (1850–2013 CE)

Changes in faunal abundance (text-fig. 8), biogenic silica and shell geochemistry (text-fig. 9) during the most recent 150 years are substantial, and align more synchronously than do changes at any other time during the previous ~1850-year records.

At 1850 CE, the Mackenzie River mean outflow starts declining from a high point (11,693 m³/s), so that by 1950 CE, it reaches a low of 7,204 m³/s, outside of standard deviation ranges (text-fig. 9d; Wickert, 2016). In addition, around 1850 CE, sharp declines in biogenic silica and the carbonate δ^{13}C values of both analyzed species, *P. pseudopunctillata* and *C. teretis* s.l., are evidence for reduced water column productivity. *C. reniforme* (71%) reached its highest abundance with *E. clavatum* (28%) and *P. pseudopunctillata* (~60%) both responding to cold shelf waters and detrital or terrestrial carbon food sources (lower carbonate δ^{13}C values). From 1850 to 1900 CE, the δ^{18}O of both *P. pseudopunctillata* and *C. teretis* s.l. increased by 0.5‰ above standard deviation ranges, which supports not only reduced freshwater mixing from lower Mackenzie River discharge but continued cooling of 1-2°C to ~1900 CE, the coldest interval of the record. Cooling until 1900 CE agrees with the summer Arctic temperature reconstruction of Kaufman et al. (2009), which was particularly evident in records from ice and lakes in northern Canada and Greenland. Our
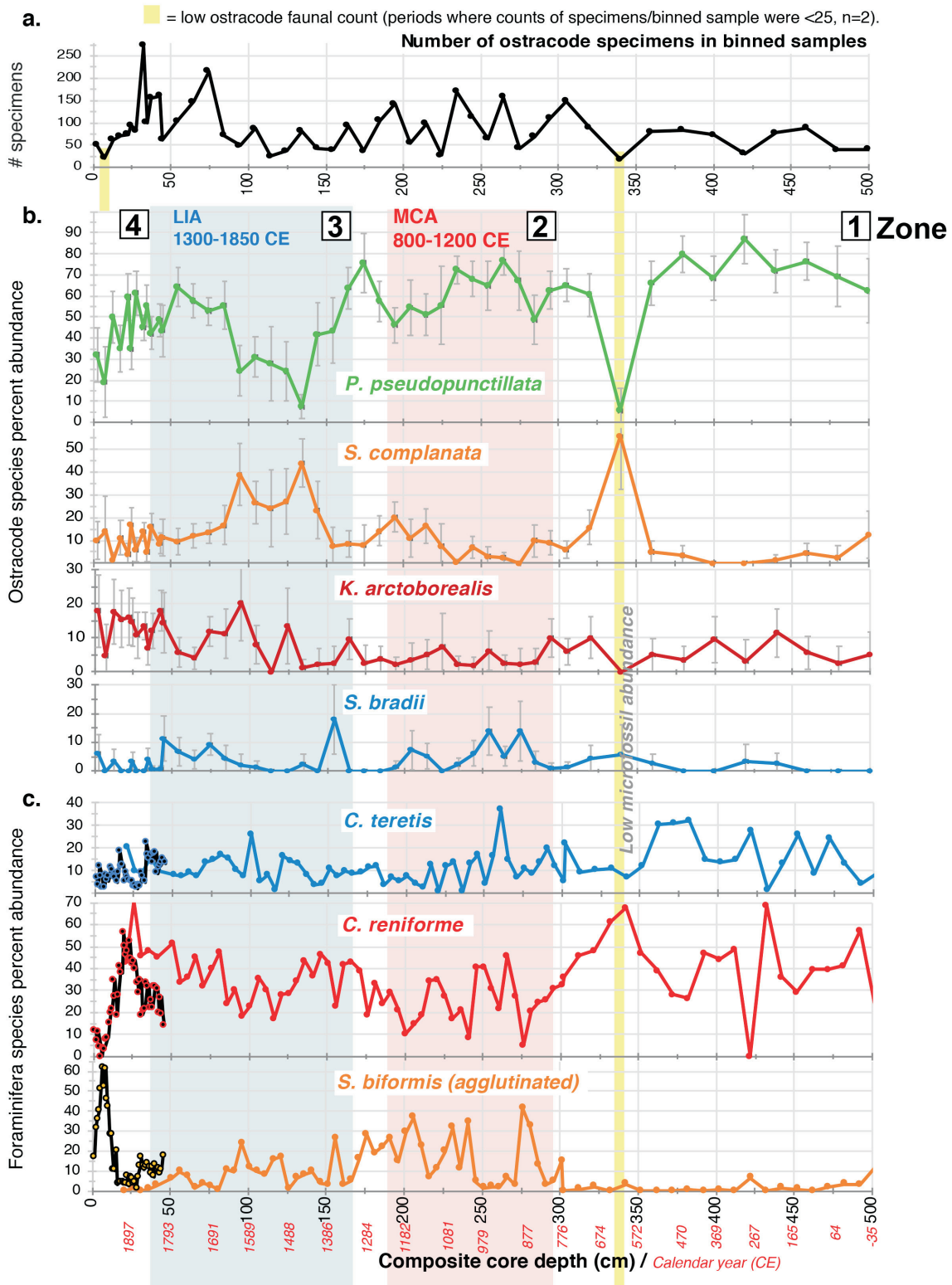
TEXT-FIGURE 8

a) Number of ostracode specimens per binned sample; MC29 was binned every 5 cm, GGC30 every 10 cm and JPC32 every 20 cm. Two samples contained <25 specimens/binned sample, and these are indicated by yellow highlights. b) Percent abundance of selected benthic ostracode and c) foraminifera species (of total specimens/sample) against composite core depth. Selected foraminifera faunal data from Seidenstein et al (2018). Foraminifera species abundance in MC29 (black lines) are plotted separately from GGC30/JPC32. General periods of the LIA (1300–1850; ~36–160 cm composite depth) and MCA (800–1200; 195–294 cm), per our age model, are shown by blue and red shaded vertical bars, respectively. The beginning of each time zone is labeled 1, 2, 3, and 4. Confidence limits (95%) shown on the faunal plots were calculated using the algorithm for binomial probability (Raup 1991).

record shows that this 50-year cooling coincides with a steep reduction in biogenic silica and lower (or more negative) δ^{13}C values in carbonates in the microfossils, which is consistent with an increase in sea ice cover and a decrease in primary production. Enhanced sea ice during this period is also supported by diatom and dinocyst assemblage evidence in the Chukchi and Beaufort Seas (de Vernal et al. 2013; Ledu et al. 2008; Bringué and Rochon, 2012; Pieńkowski et al. 2017).

From ~1900 to 2013 CE, ostracode and foraminiferal community composition, biogenic silica and stable isotope values all displayed large changes, suggesting an important shift in water mass conditions. The proportion of dominant species *P. pseudopunctillata* begins a gradual decline, which is accompanied by a rise in *K. arctoborealis* (11–18%), *A. dunelmensis* (7–13%) and *Cytheropteron* species. The ostracode PCA (text-fig. 5a) particularly highlights this subtle increase of typical polar shelf water species *K. arctoborealis* and *A. dunelmensis* in the modern (post-1950 CE) samples, which is not otherwise clearly evident. Dominant foraminifera *C. reniforme* and *E. clavatum* follow the same declining pattern as *P. pseudopunctillata*. By 1950 CE, these species are largely replaced by agglutinated species *S. biformis* (42–62%), and *S. earlandi* (5–14%), which are associated with cold, low-salinity Arctic water and sometimes less hospitable (e.g. turbid, acidified or low oxygen) environments (Schröder-Adams et al. 1990; Jennings and Helgadottir 1994; Korsun and Hald 2000; Perner et al. 2012, 2015). Productivity, inferred from biogenic silica values, rebounds from depressed values between 1850-1900 CE to high levels above average standard deviation values from 1920 to 2013 CE, which suggests diminished sea ice and prolonged summer open waters with sufficient nutrients in the upper water column. This is supported by observations that the ice-free ocean area of the Beaufort Sea in summer has increased by 70% compared to the reference climatology (1981–2010; Wood et al. 2015). After 1900 CE, our record shows slightly higher than average δ^{18}O and δ^{13}C values in biogenic carbonates, suggesting that bottom waters remained cold with a high flux of organic matter to the seafloor due to more productive waters. High primary productivity could lead to high pCO2, and carbonate dissolution in the sediments from organic matter decay. The drastic change of microfossil species composition, reflected in the PCAs (Fig 5a,b) and rise of agglutinated species from 1950 to 1990 is an unambiguous sign that bottom waters became less hospitable for calcareous species. This inhospitality could manifest as acidic or corrosive conditions or possibly, turbidity from upwelling and/or downwelling that resuspended sediments or terrestrial inputs from Mackenzie River discharge (Kipp et al. 2018). The Mackenzie River delivers large amounts (~125 Mt/yr) of sediment to the shelf (Macdonald et al. 1998). Since 2003, freshwater discharge from the Mackenzie River has increased by 25% and particulate (terrestrial suspended particles and organic carbon) export from the Mackenzie River into the Beaufort Sea has increased by 50% (Doxaran et al. 2015).

After 1990 CE, there are signs of some recovery of calcareous species. Foraminifera showing significant increases in abundance since ~2000 CE include *Elphidium incertum* (12%) and *Elphidium bartletti* (8%), both of which prefer riverine-influenced habitats with sandy, shallow seafloor areas downstream of estuaries (Polyak et al. 2002). A strong increase in arctic summer temperature during the last ~100 years is evident in terrestrial archives (Kaufman et al. 2009). This pattern could support an increase in primary productivity and/or a longer growing season (Arrigo et al. 2008) as well. Considered in sum, the proxy records imply a dramatic change post-1900 CE in the benthic environment, which may include nutrient and carbon cycling over the Beaufort continental shelf influenced by the Mackenzie River discharge.

CONCLUSIONS

This study improves our understanding of late Holocene oceanographic changes on the Mackenzie Shelf based on benthic foraminifera (Seidenstein et al. 2018) and benthic ostracode distributions, oxygen and carbon isotope values of their shells, radiocarbon and radiometric dating and biogenic silica measurements of the sediments. Our results revealed the following:

• PCAs distinguish microfossil assemblage groupings that reflect changes in the bottom water environment particularly during 1950-2013 CE, attributed to anthropogenic influences.

• Oxygen isotope shifts appear to be correlated to the LIA, MCA, and recent periods that indicate significant alterations in bottom water mass properties. Increases in δ^{18}O reflect a ~1-2 °C decrease in temperature from the MCA to the end of the LIA.

• Comparison of δ^{18}O of *P. pseudopunctillata* in this downcore study with calibrations from modern specimens in the Bering and Chukchi Seas (Gemery et al. 2022) indicates that mixing of river water lowers the overall δ^{18}O of bottom water masses on the Mackenzie Shelf due to the proximity to the river estuary.

• From 0 to 800 CE, microfossil faunal assemblage composition, δ^{18}O and δ^{13}C records generally reflect cold conditions with multidecadal variability and some sustained Atlantic water incursions onto the shelf. Average to high biogenic silica measurements suggest productivity was fairly stable. An anomalous interval at ~600 CE of low microfossil abundance limits interpretation.

• From 800 to 1200 C, microfossil δ^{18}O suggest summer warming oscillations and periods of low productivity (biogenic silica) during the MCA, and pronounced increases in agglutinated species *S. biformis* suggest some instability (e.g. episodic food and/or turbidity) affected the bottom environment.

• From 1300 to 1600 CE, the early LIA period is marked by previously dominant *P. pseudopunctillata* declining to its lowest abundance of the record (10–30%). This suggests a period of increased current flow that winnowed its preferred fine sediment substrate. Known to inhabit sandy sediments, *S. complanata* and *K. arctoborealis* increase during this interval.

• During the mid-to-late LIA (1600–1850 CE) the abundance of *P. pseudopunctillata* rebounds with the progression of more stable, cold conditions, as indicated by high biogenic silica values and generally high δ^{18}O.

• From 1850 to 1900 CE, alignments of very high microfossil δ^{18}O, very low biogenic silica and low δ^{13}C shell carbonate values indicate this was the coldest interval of the record, characterized by enhanced sea ice that depressed primary productivity. The continuation of cold temperatures from 1850 to 1900 CE is consistent with the summer temperature reconstruction of Kaufman et al. (2009).
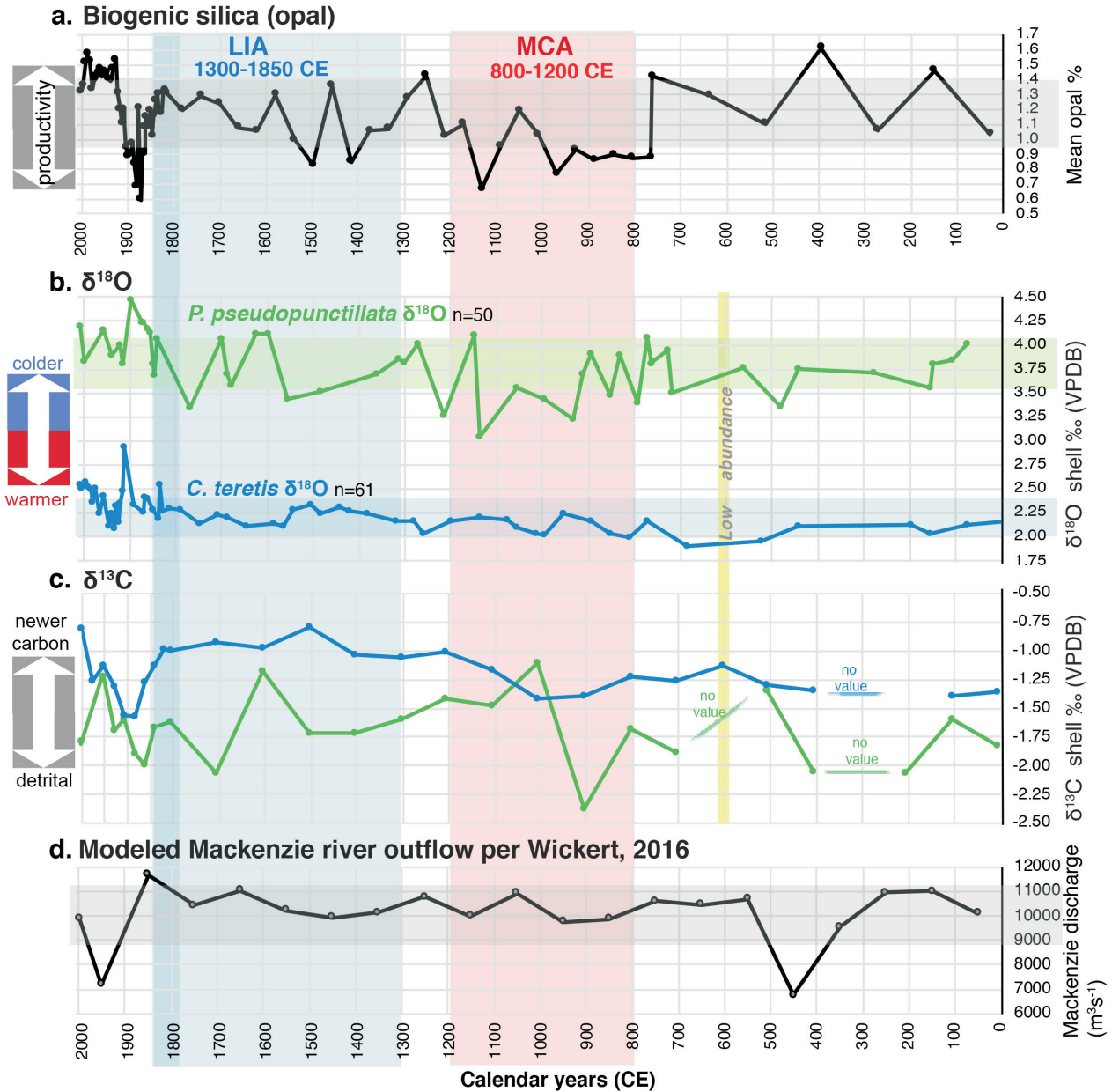
TEXT-FIGURE 9
a) Percent of sediment biogenic silica against age (calendar years, CE); b) Measurements of ostracode δ^{18}O (green) and foraminifera δ^{18}O (blue) against age; c) Measurements of ostracode δ^{13}C (green) and foraminifera δ^{13}C (blue) against age. Carbon isotope values are binned (averaged) in 25-year intervals from 1800 to 2013 and binned by 100-year intervals from 0 to 1800 CE to smooth the large variability of measured values; d) Modeled Mackenzie River outflow per Wickert (2016), and modern value representing 1990s from Carson et al. (1998). Shaded horizontal bars on plots indicate average standard deviation values.

• From 1900 to ~1990, productivity, as reflected by silica and δ^{13}C, steeply rebounds and remains high. Dominant species *P. pseudopunctillata* and *C. reniforme* decline while agglutinated taxa *S. biformis* and *S. earlandi* increase from 1950 to ~1990 to form up to 66% of the assemblage. The near-replacement of calcareous to agglutinated taxa during 1950 to ~1990 CE reflects bottom conditions more conducive to the ecology of agglutinated taxa.

• After 1990 CE, biogenic silica concentrations and δ^{18}O values remain high, and there are signs of a slight recovery of calcareous foraminifera, which notably include species whose distribution reflects river inputs, *Elphidium incertum* and *Elphidium bartletti*.

• Changes within the last ~60 years in all investigated proxies suggest longer periods of open water, high productivity, greater freshwater inputs and/or turbidity along the Canadian Beaufort Sea shelf.

DATA AVAILABILITY

ACKNOWLEDGMENTS

REFERENCES

AAGAARD, K. K., 1984. The Beaufort Undercurrent. In: Barnes, P. W., Schell, D. M., and Reimnitz, E., Eds. *The Alaskan Beaufort Sea: Ecosystems and environments*. New York: Academic Press, pp. 47–71.

ADDISON, J. A., FINNEY, B. P., JAEGER, J. M., STONER, J. S., NORRIS, R. D. and HANGSTERFER, A., 2013. Integrating satellite observations and modern climate measurements with the recent sedimentary record: An example from Southeast Alaska. *Journal of Geophysical Research: Oceans,* 118: 3444–3461.

ALLEY, R. B., AGUSTSDOTTIR, A. M. and FAWCETT, P. J., 1999. Ice-core evidence of late-Holocene reduction in North Atlantic Ocean heat transport. *Geophysical Monograph,* 112: 301–312.

AMMANN, C. M., JOOS, F., SCHIMEL, D. S., OTTO-BLIESNER, B. L. and TOMAS, R. A., 2007. Solar influence on climate during the past millennium: results from transient simulations with the NCAR Climate System Model. *Proceedings of the National Academy of Sciences of the United States of America,* 104 (10): 3713-8. doi: 10.1073/pnas.0605064103

ANDERSON, R. K., MILLER, G. H., BRINER, J. P., LIFTON, N. A. and DEVOGEL, S. B., 2008. A millennial perspective on Arctic warming from 14C in quartz and plants emerging from beneath ice caps. *Geophysical Research Letters,* 35: L01502.

ATHERSUCH, J., HORNE, D. J. and WHITTAKER, J. E., 1989. Marine and brackish water ostracods. *Synopses of the British Fauna* (New Series), 43. Leiden: E. J. Brill, 343 pp.

ARRIGO, K. R., VAN DIJKEN, G. and PABI, S., 2008. Impact of a shrinking Arctic ice cover on marine primary production. *Geophysical Research Letters,* 35: L19603.

AVERY, S. V., 1996. Fate of caesium in the environment: Distribution between the abiotic and biotic components of aquatic and terrestrial ecosystems. *Journal of Environmental Radioactivity,* 30: 139–171.

BEER, J., 2000. Long-term indirect indices of solar variability. *Space Science Reviews,* 94 (1): 53–66.

BRADLEY, R. S., BRIFFA, K. R., COLE, J., HUGHES, M. K. and OSBORN, T. J., 2003a. *The climate of the last millennium.* In: Alverson, K. D., Bradley, R.S. and Pedersen, T.F., Eds., *Paleoclimate, Global Change and the Future*. Berlin: Springer Verlag, 105–141.

BRADLEY, R. S., HUGHES, M. K. and DIAZ, H. F., 2003b. Climate in Medieval time. *Science,* 302: 404–405.

BRINGUÉ, M. and ROCHON, A., 2012. Late Holocene paleoceanography and climate variability over the Mackenzie slope (Beaufort Sea, Canadian Arctic). *Marine Geology,* 291-294: 83–96.

BROECKER, W. S., 2001. Was the Medieval warm period global? *Science,* 291 (5508): 1497–1499.

BROUWERS, E. M., CRONIN, T. M., HORNE, D. J., LORD, A. R., 2000. Recent shallow marine ostracods from high latitudes: Implications for late Pliocene and Quaternary palaeoclimatology. *Boreas,* 29 (2): 127–142.

BUZAS, M. A., CULVER, S. J. and JORISSEN, F. J., 1993. A statistical evaluation of the microhabitats of living (stained) infaunal benthic foraminifera. *Marine Micropaleontology,* 20: 311–320.

CAGE, A. G., PIEŃKOWSKI, A. J., JENNINGS, A., KNUDSEN, K. L. and SEIDENKRANTZ, M.-S., 2021. Comparative analysis of six common foraminiferal species of the genera *Cassidulina, Paracassidulina*, and *Islandiella* from the Arctic–North Atlantic domain. *Journal of Micropalaeontology,* 40: 37–60. https://doi.org/10.5194/jm-40-37-2021

CARMACK, E. C. and KULIKOV, E. A., 1998. Wind-forced upwelling and internal Kelvin wave generation in Mackenzie Canyon, Beaufort Sea. *Journal of Geophysical Research,* 103 (C9): 18,447–18,458.

CARMACK, E. C. and MACDONALD, R. W., 2002. Oceanography of the Canadian Shelf of the Beaufort Sea: A Setting for Marine Life. *Arctic,* 55: 29–45.

CARMACK, E. C., MACDONALD, R. W. and JASPER, S., 2004. Phytoplankton productivity on the Canadian Shelf of the Beaufort Sea. *Marine Ecology Progress Series,* 277: 37–50.

CARMACK, E. C., MACDONALD, R. W. and PAPADAKIS, J. E., 1989. Water mass structure and boundaries in the Mackenzie shelf estuary. *Journal of Geophysical Research,* 94 (C12): 18,043–18,055.

CARSON, M. A., JASPER, J. N. and CONLY, F.M., 1998. Magnitude and sources of sediment input to the Mackenzie Delta, Northwest Territories, 1974–94. *Arctic,* 51: 116–124.

COOPER, L. W., GREBMEIER, J. M., LARSEN, I. L., DOLVIN, S. and REED, A. J., 1998. Inventories and distribution of radiocaesium in arctic marine sediments: influence of biological and physical processes. *Chemistry and Ecology,* 15: 27–46.

COMISO, J. C., MEIER, W. N. and GERSTEN, R., 2017. Variability and trends in the Arctic Sea ice cover: results from different techniques. *Journal of Geophysical Research,* 122: 6883–6900.

COPLEN, T. P., 1994. Reporting of stable hydrogen, carbon, and oxygen isotopic abundance. *Pure and Applied Chemistry,* 66: 273–276.

CRAIG, H., 1961. Standard for reporting concentrations of deuterium and oxygen-18 in natural waters. *Science,* 133: 1833–1834.

CRONIN, T. M., 1977. Late-Wisconsin Marine Environments of the Champlain Valley (New York, Quebec). *Quaternary Research,* 7: 238–253.

CRONIN, T. M., HOLTZ, T. R., and WHATLEY, R. C., 1994. Quaternary paleoceanography of the deep Arctic Ocean based on quantitative analysis of Ostracoda. *Marine Geology,* 119: 305–332.

CRONIN, T. M., GEMERY, L., BRIGGS JR., W. M., JAKOBSSON, M., POLYAK, L. and BROUWERS, E. M., 2010. Quaternary sea-ice history in the Arctic Ocean based on a new ostracode sea-ice proxy. *Quaternary Science Reviews,* 29: 3415–3429.

CRONIN, T. M., GEMERY, L., BRIGGS, JR., W. M., BROUWERS, E. M., SCHORNIKOV, E. I., STEPANOVA, A., WOOD, A., YASUHARA, M. and SIU, S., 2021. Arctic Ostracode Database 2020. NOAA's National Centers for Environmental Information (NCEI). Available at https://www.ncdc.noaa.gov/paleo/study/32312

CROWLEY, T. J., 2000. Causes of climate change over the past 1000 years. *Science,* 289: 270–277.

DE VERNAL, A., HILLAIRE-MARCEL, C. and DARBY, D., 2005. Variability of sea ice cover in the Chukchi Sea (western Arctic Ocean) during the Holocene. *Paleoceanography,* 20: PA4018.

DE VERNAL, A., HILLAIRE-MARCEL, C., ROCHON, A., FRÉCH-ETTE, B., HENRY, M., SOLIGNAC, S. and BONNET, S., 2013. Dinocyst-based reconstructions of sea ice cover concentration during the Holocene in the Arctic Ocean, the northern North Atlantic Ocean and its adjacent seas. *Quaternary Science Reviews,* 79: 111–121.

DOXARAN, D., DEVRED, E. and BABIN, M., 2015. A 50% increase in the mass of terrestrial particles delivered by the Mackenzie River into the Beaufort Sea (Canadian Arctic Ocean) over the last 10 years. *Biogeosciences,* 12: 3551–3565. https://doi.org/10.5194/bg-12-3551-2015

ELOFSON, O., 1941. Zur Kenntnis der marinen Ostracoden Schwedens mit besonderer Berucksichtigung des Skageraks. *Zoologiska Bidrag fran Uppsala*, 19: 215–534.

FARMER, J. R., CRONIN, T. M., DE VERNAL, A., DWYER, G. S., KEIGWIN, L. D. and THUNELL, R. C., 2011. Western Arctic Ocean temperature variability during the last 8000 years. *Geophysical Research Letters,* 38: L24602.

FOUKAL, N. P., PICKART, R. S., MOORE, G. and LIN, P., 2019. Shelfbreak downwelling in the Alaskan Beaufort Sea. *Journal of Geophysical Research: Oceans,* 124 (10): 7201–7225.

FREIWALD, A. and MOSTAFAWI, N., 1998. Ostracods in a cold-temperate coastal environment, western Troms, northern Norway: Sedimentary aspects and assemblages. *Facies,* 38: 255–274

FREY, K. E., MOORE, G. W. K., COOPER, L. W. and GREBMEIER, J. M., 2015. Divergent patterns of recent sea ice cover across the Bering, Chukchi and Beaufort seas of the Pacific Arctic Region. *Progress in Oceanography,* 136: 32–49.

GEMERY, L., 2021. Data release to multi-proxy record of ocean-climate variability during the last 2 millennia on the Mackenzie Shelf, Beaufort Sea. U.S. Geological Survey data release. https://doi.org/10.5066/P9SRRW6T

GEMERY, L., CRONIN, T. M., COOPER, L. W., DOWSETT, H. J. and GREBMEIER, J. M., 2021. Biogeography and Ecology of Ostracoda in the U.S. northern Bering, Chukchi, and Beaufort Seas. *PLOS One*. https://doi.org/10.1371/journal.pone.0251164

GEMERY, L., COOPER, L. W., MAGEN, C., CRONIN, T. M. and GREBMEIER, J. M., 2022. Stable oxygen isotopes in shallow marine ostracodes from the northern Bering and Chukchi Seas. *Marine Micropaleontology*, 174: 102001.

GEMERY L., CRONIN T. M., POIRIER, R. K., PEARCE C., BARRIENTOS, N., O'REGAN, M., JOHANSSON, C., KOSHURNIKOV, A. and JAKOBSSON, M., 2017. Central Arctic Ocean paleoceanography from ~50 ka to present, on the basis of ostracode faunal assemblages from SWERUS 2014 expedition. *Climate of the Past*. https://doi.org/10.5194/cp-2017-22

GEMERY, L., CRONIN, T. M., BRIGGS, W. M., BROUWERS, E. M., SCHORNIKOV, E., STEPANOVA, A., WOOD, A. M. and YASUHARA, M., 2015. An Arctic and subarctic ostracode database: biogeographic and paleoceanographic applications. *Hydrobiologia,* 786 (1): 59–95.

GEOMAPAPP [Internet] Available from http://www.geomapapp.org/index.htm

GOOSSE, H., RENSSEN, H., TIMMERMANN, A. and BRADLEY, R. A., 2005. Internal and forced climate variability during the last millennium — a model-data comparison using ensemble simulations. *Quaternary Science Reviews,* 24: 1345–1360.

GREBMEIER, J. M, COOPER, L. W., ASHJIAN, C. A., BLUHM, B. A., CAMPBELL, R. B., DUNTON, K. E., MOORE, J., OKKONEN, S., SHEFFIELD, G., TREFRY, J. and PASTERNAK, S. Y., 2015. Pacific Marine Arctic Regional Synthesis (PacMARS) Final Report, North Pacific Research Board, 259 pp.

HALD, M., STEINSUND, P. I., DOKKEN, T., KORSUN, S., POLYAK, L. and ASPELI, R., 1994. Recent and late Quaternary distribution of *E. excavatum forma clavata* in Arctic seas. *Cushman Foundation Special Publication,* 32: 141–153.

HAMMER, Ø., HARPER, D. A. T. and RYAN, P. D., 2001. PAST: Paleontological statistics software package for education and data analysis. *Palaeontologia Electronica,* 4 (1): 9.

HAYWARD, B. W., GRENFELL, H. R., SAVAA, A. T. and DAYMOND-KING, R., 2007. Biogeography and ecological distribution of shallow-water benthic foraminifera from the Auckland and Campbell Islands, subantarctic southwest Pacific. *Journal of Micropalaeontology,* 26: 127–143.

HAZEL, J. E., 1970. Atlantic continental shelf and slope of the United States: ostracode zoogeography in the southern Nova Scotian and northern Virginian faunal provinces. *U.S. Geological Survey Professional Paper,* 529-E: 1–21.

HEATON T. J., KÖHLER, P., BUTZIN, M., BARD, E., REIMER, R. W., AUSTIN, W. E. N., BRONK RAMSEY, C., HUGHEN, K. A., KROMER, B., REIMER, P. J., ADKINS, J., BURKE, A., COOK, M. S., OLSEN, J. and SKINNER, L. C., 2020. Marine20 – the marine radiocarbon age calibration curve (0-55,000 cal BP). *Radiocarbon,* 62: doi: 10.1017/RDC.2020.68.

HOLMES, J. A. and CHIVAS, A. R., 2002. Ostracod shell chemistry — Overview. In: Holmes, J.A. and Chivas, A. R., Eds., The Ostracoda: applications in Quaternary Research. *Geophysical Monograph Series*, 131: 185–204, AGU, Washington, D.C. https://doi.org/10.1029/131GM10

HORNE, D. J., 1983. Life-cycles of podocopid Ostracoda - a review (with particular reference to marine and brackish-water species). In: Maddocks, R., Ed., Applications of Ostracoda. Proceedings of the Eighth International Symposium on Ostracoda. University of Houston, Dept. of Geosciences, Houston, Texas, pp. 581–590.

HÖRNER, T., STEIN, R., FAHL, K. and BIRGEL, D., 2016. Post-glacial variability of sea ice cover, river run-off and biological production in the western Laptev Sea (Arctic Ocean)–A high-resolution biomarker study. *Quaternary Science Reviews,* 143: 133–149.

INTERGOVERNMENTAL PANEL ON CLIMATE CHANGE (IPCC)., 2021. Contribution of Working Group I to the Sixth Assessment Report of the Intergovernmental Panel on Climate Change. In: Masson-Delmotte, V., P. Zhai, A. Pirani, S. L. Connors, C. Peìan, S. Berger, N. Caud, Y. Chen, L. Goldfarb, M. I. Gomis, M. Huang, K. Leitzell, E. Lonnoy, J. B. R. Matthews, T. K. Maycock, T. Waterfield, O. Yelekc, I. R. Yu and B. Zhou, Eds., *Climate Change 2021: The Physical Science Basis.* Cambridge University Press. https://www.ipcc.ch/report/ar6/wg1/#FullReport

ISHMAN, S. E. and FOLEY, K. M., 1996. Modern benthic foraminifer distribution in the Amerasian Basin, Arctic Ocean. *Micropaleontology,* 42 (2): 206–220.

JACKSON, J. M., MELLING, H., LUKOVICH, J. V., FISSEL, D. and BARBER, D. G., 2015. Formation of winter water on the Canadian Beaufort shelf: New insight from observations during 2009–2011. *Journal of Geophysical Research: Oceans,* 120: 4090–4107.

JAKOBSSON, M., MAYER, L., COAKLEY, B., DOWDESWELL, J. A., FORBES, S., FRIDMAN, B., HODNESDAL, H., NOORMETS, R., PEDERSEN, R., REBESCO, M., SCHENKE, H. W., ZARAYSKAYA, Y., ACCETTELLA, D., ARMSTRONG, A., ANDERSON, R. M., BIENHOFF, P., CAMERLENGHI, A., CHURCH, I., EDWARDS, M., GARDNER, J. V., HALL, J. K., HELL, B., HESTVIK, O., KRISTOFFERSEN, Y., MARCUSSEN, C., MOHAMMAD, R., MOSHER, D., NGHIEM, S. V., PEDROSA, M. T., TRAVAGLINI, P. G. and WEATHERALL, P., 2012. The International Bathymetric Chart of the Arctic Ocean (IBCAO) Version 3.0. *Geophysical Research Letters,* 39 (12): L12609. https://doi.org/10.1029/2012GL052219

JENNINGS, A. E. and HELGADOTTIR, G., 1994. Foraminiferal assemblages from the fjords and shelf of eastern Greenland. *Journal for Foraminiferal Research,* 24 (2): 123–144.

KAUFMAN, D. S., SCHNEIDER, D. P., MCKAY, N. P., AMMANN, C. M., BRADLEY, R. S., BRIFFA, K. R., MILLER, G. H., OTTO-BLIESNER, B. L., OVERPECK, J. T. and VINTHER, B. M., 2014. Arctic Lakes 2k Project Members, 2009. Recent warming reverses long-term Arctic cooling. *Science,* 235: 1236–1239.

KIPP, L. E., CHARETTE, M. A., MOORE, W. S., HENDERSON, P. B. and RIGOR, I. G., 2018. Increased fluxes of shelf-derived materials to the central Arctic Ocean. *Science Advances,* 4: eaao1302. https://doi.org/10.1126/sciadv.aao1302

KORSUN, S. and HALD, M., 2000. Seasonal dynamics of benthic foraminifera in a glacially fed fjord of Svalbard, European Arctic. *Journal of Foraminiferal Research,* 30 (4): 251–271.

KULIKOV, E., CARMACK, E. and MACDONALD, R., 1998. Flow variability at the continental shelf break of the Mackenzie Shelf in the Beaufort Sea. *Journal of Geophysical Research: Oceans,* 103: 12725–12741.

LAZAR, K. B., POLYAK, L. and DIPRE, G. R., 2016. Re-examination of the use of *Cassidulina neoteretis* as a Pleistocene biostratigraphic marker in the Arctic Ocean. *Journal of Foraminiferal Research,* 46 (2): 115–123.

LEDU, D., ROCHON, A., DE VERNAL, A. and ST-ONGE, G., 2008. Palynological evidence of Holocene climate change in the eastern Arctic: a possible shift in the Arctic Oscillation at the millennial time scale. *Canadian Journal of Earth Sciences,* 45 (11): 1363–1375.

——, Holocene sea-ice history and climate variability along the main axis of the Northwest Passage. Canadian Arctic. *Paleoceanography,* 25: PA2213.

——, Holocene paleoceanography of the Northwest Passage, Canadian Arctic Archipelago. *Quaternary Science Reviews,* 29: 3468–3488.

LIN, P., PICKART, R. S., FISSEL, D. B., BORG, K., MELLING, H. and WIESE, F. K., 2021. On the nature of wind-forced upwelling and downwelling in Mackenzie Canyon, Beaufort Sea. *Progress in Oceanography,* 198: 102674.

LIN, P., PICKART, R. S., FISSEL, D., ROSS, E., KASPER, J., BAHR, F., TORRES, D. J., O'BRIEN, J., BORG, K. and MELLING, H., 2020. Circulation in the vicinity of Mackenzie Canyon from a year-long mooring array. *Progress in Oceanography,* 187: 102396. https://doi.org/10.1016/j.pocean.2020.102

LIN, P., PICKART, R. S., MCRAVEN, L. T., ARRIGO, K. R., BAHR, F., LOWRY, K. E., STOCKWELL, D. A. and MORDY, C. W., 2019a. Water mass evolution and circulation of the northeastern Chukchi Sea in summer: Implications for nutrient distributions. *Journal of Geophysical Research: Oceans,* 127 (7): 4416–4432.

LIN, P., PICKART, R. S., MOORE, G. W. K., SPALL, M. A. and HU, J., 2019b. Characteristics and dynamics of wind-driven upwelling in the Alaskan Beaufort Sea based on six years of mooring data. Deep Sea Research Part II: *Topical Studies in Oceanography,* 124 (7): 4416–4432.

MACDONALD, R. W., WONG C. S. and ERICKSON, P. E., 1987. The distribution of nutrients in the southeastern Beaufort Sea: Implications for water circulation and primary production. *Journal of Geophysical Research,* 92: 2939–2952.

MACDONALD, R. W., CARMACK, E. C., MCLAUGHLIN, F. A., ISEKI, K., MACDONALD, D. M. and O'BRIEN, M. C., 1989. Composition and modification of water masses in the Mackenzie Shelf Estuary. *Journal of Geophysical Research,* 94 (C12): 18057–18070.

MACKENSEN, A. and HALD, M., 1988. *Cassidulina teretis* Tappan and *C. laevigata* d'Orbigny: Their modern and late Quaternary distribution in northern seas. *Journal of Foraminiferal Research,* 18: 16–24.

MACKENSEN, A., SCHUMACHER, S., RADKE, J. and SCHMIDT, D. N., 2000. Microhabitat preferences and stable carbon isotopes of endobenthic foraminifera: Clue to quantitative reconstruction of oceanic new production? *Marine Micropaleontology,* 40: 233–258.

MANN, M. E., ZHANG, A., HUGHES, M. K., BRADLEY, R. S., MILLER, S. K., RUTHERFORD, S. and NI, F., 2008. Proxy-based reconstructions of hemispheric and global surface temperature variations over the past two millennia. *Proceedings of the National Academy of Sciences,* 105, 13252–13257.

MCKAY, N. and KAUFMAN, D., 2014. An extended Arctic proxy temperature database for the past 2,000 years. *Scientific Data* 1: 140026. https://doi.org/10.1038/sdata.2014.26

MELLING, H., 2000. Exchanges of freshwater through the shallow straits of the North American Arctic. In Lewis, E. L., Jones, E. P., Lemke, P., Prowse, T. D. and Wadhams, P., Eds., *The Freshwater Budget of the Arctic Ocean*, 479–502. Dordrecht: Springer.

MELLING, H. and RIEDEL, D. A., 1996. Development of seasonal pack ice in the Beaufort Sea during the winter of 1991– 92: A view from below. *Journal of Geophysical Research,* 101: 11975–11992.

MORTLOCK, R. A. and FROEHLICH, P. N., 1989. A simple method for the rapid determination of biogenic opal in pelagic marine sediments. *Deep-Sea Research,* 36 (9): 1415–1426.

MILLER, G. H., BRIGHAM-GRETTE, J., ALLEY, R. B., ANDERSON, L., BAUCH, H. A., DOUGLAS, M. S. V., EDWARDS, M. E., ELIAS, S. A., FINNEY, B. P., FITZPATRICK, J. J., FUNDER, S. V., HERBERT, T. D., HINZMAN, L. D., KAUFMAN, D. S., MACDONALD, G. M., POLYAK, L., ROBOCK, A., SERREZE, M. C., SMOL, J. P., SPILHAGEN, R., WHITE, J. W. C., WOLFE, A. P. and WOLFF, E. W., 2010. Temperature and precipitation history of the Arctic. *Quaternary Science Review,* 29 (15-16): 1679–1715.

NEALE, J. W. and HOWE, H. V., 1975. The marine Ostracoda of Russian Harbour, Novaya Zemlya and other high latitude faunas. *Bulletin of American Paleontology,* 65 (282): 381–431.

NIKOLOPOULOS, A., PICKART, R. S., FRATANTONI, P. S., SHIMADA, K., TORRES, D. J. and JONES, E. P., 2009. The western Arctic boundary current at 152°W: Structure, variability, and transport. *Deep Sea Research Part II,* 56: 1164–1181.

OKAZAKI, Y., TAKAHASHI, K., ASAHI, H., KATSUKI, K., HORI, J., YASUDA, H., SAGAWA, Y. and TOKUYAMA, H., 2005. Productivity changes in the Bering Sea during the late Quaternary. Deep-sea Research Part II: *Topical Studies in Oceanography,* 52: 2150–2162.

OKKONEN, S., 2013. CTD Summary Data. Version 1.0. UCAR/NCAR - *Earth Observing Laboratory.* https://doi.org/10.5065/D6DB7ZVJ. Accessed 30 Jul 2021.

PAGES 2K CONSORTIUM: AHMED, M. et al., 2013. Continental-scale temperature variability during the past two millennia. *Nature Geoscience,* 6: 339–346.

PEARCE, C., VARHELYI, A., WASTEGÅRD, S., MUSCHITIELLO, F., BARRIENTOS, N., O'REGAN, M., CRONIN, T. M., GEMERY, L., SEMILETOV, I., BACKMAN, J. and JAKOBSSON, M., 2017. The 3.6 ka Aniakchak tephra in the Arctic Ocean: a constraint on the Holocene radiocarbon reservoir age in the Chukchi Sea. *Climate of the Past,* 13: 303–316.

PERNER, K., MOROS, M., KUIJPERS, A., TELFORD, R. J. and HARFF, J., 2011. Centennial scale benthic foraminiferal record of late Holocene oceanographic variability in Disko Bugt, West Greenland. *Quaternary Science Reviews,* 30: 2815–2826.

PERNER, K., MOROS, M., JENNINGS, A., LLOYD, J. M. and KNUDSEN, K. L., 2013. Holocene palaeoceanographic evolution of West Greenland. *The Holocene,* 23: 374–387.

PERNER, K. MOROS, M., LLOYD, J. M., JANSEN, E. and STEIN, R., 2015. Mid to late Holocene strengthening of the East Greenland Current linked to warm subsurface Atlantic water. *Quaternary Science Reviews,* 129: 296–307.

PICKART, R.S., 2004. Shelfbreak circulation in the Alaskan Beaufort Sea: Mean structure and variability. *Journal of Geophysical Research,* 109: C04024, doi:10.1029/2003JC001912

PIEÑKOWSKI, A. J., GILL, N. K., FURZE, M. F. A., MUGO, S. M., MARRET, F. and PERREAUX, A., 2017. Arctic sea-ice proxies: Comparisons between biogeochemical and micropalaeontological reconstructions in a sediment archive from Arctic Canada. *The Holocene,* 27 (5): 665–682.

POIRIER, R. K., CRONIN, T. M., BRIGGS JR., W. M. and LOCKWOOD, R., 2012. Central Arctic paleoceanography for the last 50 kyr based on ostracode faunal assemblages. *Marine Micropaleontology,* 88–89: 65–76.

POLYAK, L., KORSUN, S., FEBO, L.A., STANOVOY, V., KHUSID, T., HALD, M., PAULSEN, B. E. and LUBINSKI, D. J., 2002. Benthic foraminiferal assemblages from the southern Kara Sea, a river-influenced arctic marine environment. *Journal of Foraminiferal Research,* 32: 252–273.

POLYAK, L. BEST, K. M., CRAWFORD, K. A., COUNCIL, E. A. and ST-ONGE, G., 2013. Quaternary history of sea ice in the western Arctic Ocean based on foraminifera. *Quaternary Science Reviews,* 79: 145–156.

POLYAK, L., BELT, S. T., CABEDO-SANZ, P., YAMAMOTO, M. and PARK, Y. H., 2016. Holocene sea-ice conditions and circulation at the Chukchi-Alaskan margin, Arctic Ocean, inferred from bio-marker proxies. *Holocene,* 26: 1810–1821.

PROSHUTINSKY, A., KRISHFIELD, R., TOOLE, J. M., TIMMERMANS, M.-L., WILLIAMS, W., ZIMMERMANN, S., YAMAMOTO-KAWAI, M., ARMITAGE, T. W. K., DUKHOVSKOY, D., GOLUBEVA, E., MANUCHARYAN, G. E., PLATOV, G., WATANABE, E., KIKUCHI T., NISHINO, S., ITOH, M., KANG, S.-H., CHO, K.-H., TATEYAMA, K. and ZHAO, J., 2019. Analysis of the Beaufort Gyre freshwater content in 2003–2018. *Journal of Geophysical Research: Oceans,* 124: 9658–9689.

RAVELO, A.C. and HILLAIRE-MARCEL, C., 2007. The use of oxygen and carbon isotopes of foraminifera in paleoceanography. *Developments in Marine Geology. Elsevier B.V.* doi:10.1016/S1572-5480(07)01023-8

RAWLINS, M. A., STEELE, M., HOLLAND, M. M., ADAM, J. C., CHERRY, J. E., FRANCIS, J. A., GROISMAN, P. Y., HINZMAN, L. D., HUNTINGTON, T. G., KANE, D. L., KIMBALL, J. S., KWOK, R., LAMMERS, R. B., LEE, C. M., LETTENMAIER, D. P., MCDONALD, K. C., PODEST, E., PUNDSACK, J. W., RUDELS, B., SERREZE, M. C., SHIKLOMANOV, A., SKAGSETH, Ø., TROY, T. J., VÖRÖSMARTY, C. J., WENSNAHAN, M., WOOD, E. F., WOODGATE, R., YANG, D., ZHANG, K. and ZHANG, T., 2010. Analysis of the Arctic system for freshwater cycle intensification: Observations and expectations. *Journal of Climate,* 23: 5715–5737.

RAUP, D. M., 1991. The future of analytical paleobiology. *Short Courses in Paleontology* 4: 207–216. doi:10.1017/S2475263000002208

ROOD, S. B., KALUTHOTA, S., PHILIPSEN, L. J., ROOD, N. J. and ZANEWICH, K. P., 2017. Increasing discharge from the Mackenzie River system to the Arctic Ocean. *Hydrological Processes,* 31: 150–160.

ROHLING, E. J. and COOKE, S., 1999. Stable oxygen and carbon isotopes in foraminiferal carbonate shells. In: Sen Gupta, B. K., Ed., *Modern foraminifera.* Dordrecht: Kluwer Academic Publishers, 239–258.

RUDELS, B., JONES, E. P., ANDERSON, L. G. and KATTNER, G., 1994. On the intermediate depth waters of the Arctic Ocean. In: Johannessen, O. M., Muench, R. D. and Overland, J. E., Eds., The Polar Oceans and Their Role in Shaping the Global Environment: The Nansen Centennial Volume. *Geophysical Monograph Series,* 85: 33–46.

SCHLITZER, R., 2018. *Ocean Data View,* https://odv.awi.de.

SCHRÖDER-ADAMS, C. J. and VAN ROOYEN, D., 2011. Response of Recent Benthic Foraminiferal Assemblages to Contrasting Environments in Baffin Bay and the Northern Labrador Sea, Northwest Atlantic. *Arctic,* 64: 317–341.

SCHRÖDER-ADAMS, C. J., COLE, F. E., MEDIOLI, P. J., SCOTT, D. B. and DOBBIN, L., 1990. Recent Arctic shelf Foraminifera– Seasonally ice covered vs. perennially ice-covered areas. *Journal of Foraminiferal Research,* 20: 8–36.

SCOTT, D.B., SCHELL, T., ROCHON, A. and BLASCO, S., 2008. Modern benthic foraminifera in the surface sediments of the Beaufort shelf, slope, and Mackenzie trough, Beaufort Sea, Canada: Taxonomy and summary of surficial distributions. *Journal of Foraminiferal Research,* 38: 228–250.

SCOTT, D. B., SCHELL, T., ST-ONGE, G., ROCHON, A. and BLASCO, S., 2009. Foraminiferal assemblage changes over the last 15,000 years on the Mackenzie-Beaufort Sea Slope and Amundsen Gulf, Canada: Implications for past sea ice conditions. *Paleoceanography,* 24: PA2219. doi:10.1029/2007PA001575

SEIDENKRANTZ, M.-S., 1995. *Cassidulina teretis* Tappan and *Cassidulina neoteretis* new species (Foraminifera): stratigraphic markers for deep sea and outer shelf areas. *Journal of Micropalaeontology,* 14: 145–157.

SEIDENSTEIN, J. L., CRONIN, T. M., GEMERY, L., KEIGWIN, L. D., PEARCE, C., JAKOBSSON, M., COXALL, H., WEI, E. and DRISCOLL, N., 2018. Late Holocene paleoceanography in the Chukchi and Beaufort Seas, Arctic Ocean, based on benthic foraminifera and ostracodes. *Arktos*. https://doi.org/10.1007/s41063-018-0058-7

SMITH, A. J. and HORNE, D. J., 2002. Ecology of marine, marginal marine and nonmarine ostracodes. In: Holmes, J. A. and Chivas, A. R., Eds., The Ostracoda: Applications in Quaternary Research, American Geophysical Union, *Geophysical Monograph,* 131: 37–64.

STEIN, R. and FAHL, K., 2000. Holocene accumulation of organic carbon at the Laptev Sea continental margin (Arctic Ocean): sources, pathways, and sinks. *Geo-Marine Letters,* 20: 27–36.

STEIN, R., FAHL, K., SCHADE, I., MANERUNG, A., WASSMUTH, S., NIESSEN, F. and NAM, S. I., 2017. Holocene variability in sea ice cover, primary production, and Pacific-Water inflow and climate change in the Chukchi and East Siberian Seas (Arctic Ocean). *Journal of Quaternary Science,* 32: 362–379.

STEPANOVA, A. Y., 2006. Late Pleistocene-Holocene and recent Ostracoda of the Laptev Sea. Monograph. Suppl. Issue Russ. *Paleontological Journal,* 40 (2): S91–S204.

STEPANOVA, A., TALDENKOVA, E. and BAUCH, H.A., 2003. Recent Ostracoda of the Laptev Sea (Arctic Siberia): taxonomic composition and some environmental implications. *Marine Micropaleontology,* 48: 23–48.

STEPANOVA, A., TALDENKOVA, E., SIMSTICH, J. and BAUCH, H. A., 2007. Comparison study of the modern ostracod associations in the Kara and Laptev seas: ecological aspects. *Marine Micropaleontology,* 63: 111–142

STEPANOVA, A., OBROCHTA, S., QUINTANA KRUPINSKI, N. B., HYTTINEN, O., KOTILAINEN, A. and ANDRÉN, T., 2019. Late Weichselian to Holocene history of the Baltic Sea as reflected in ostracod assemblages. *Boreas,* 48: 761–778.

STUIVER, M., REIMER, P. J. and REIMER, R.W., 2021. CALIB 8.2 [WWW program] at http://calib.org. Accessed 2021-1-26.

STRANNE, C., JAKOBSSON, M. and BJÖRK, G., 2014. Arctic Ocean perennial sea ice breakdown during the Early Holocene Insolation Maximum. *Quaternary Science Reviews,* 92: 123–132.

TAPPAN, H., 1951. Northern Alaska index foraminifera. *Contributions from the Cushman Foundation for Foraminiferal Research,* 2: 1–8.

TIMMERMANS, M.-L., TOOLE, J. and KRISHFIELD, R., 2018. Warming of the interior Arctic Ocean linked to sea ice losses at the basin margins. *Science Advances,* 4 (8): eaat6773. doi:10.1126/sciadv.aat6773

YAMAMOTO, M., NAM, S. I., POLYAK, L., KOBAYASHI, D., SUZUKI, K., IRINO, T. and SHIMADA, K., 2016. Holocene dynamics in the Bering Strait inflow to the Arctic and the Beaufort Gyre circulation based on sedimentary records from the Chukchi Sea. *Climate of the Past,* 13 (9): 1111–1127.

VAN DIJK, I., BERNHARD, J.M., DE NOOIJER, L.J., NEHRKE, G., WIT, J.C. and REICHART, G.J., 2017. Combined impacts of ocean acidification and dysoxia on survival and growth of four agglutinated foraminifera. *Journal of Foraminiferal Research,* 47 (3): 294–303.

VON APPEN, W.-J. and PICKART, R. S., 2012. Two configurations of the western Arctic shelfbreak current in summer. *Journal of Physical Oceanography,* 42 (3): 329–351.

VON GRAFENSTEIN, U., ERLERNKEUSER, H. and TRIMBORN, P., 1999. Oxygen and carbon isotopes in modern freshwater ostracod valves: assessing vital offsets and autecological effects of interest for palaeoclimate studies. *Palaeogeography, Palaeoclimatology, Palaeoecology,* 148: 133–152.

WEINGARTNER, T., AAGAARD, K., WOODGATE, R., DANIELSON, S., SASAKI, Y. and CAVALIERI, D., 2005. Circulation on the north central Chukchi Sea shelf. *Deep Sea Research Part II,* 52 (24-26): 3150–3174.

WEINGARTNER, T. J., CAVALIERI, D. J., AAGAARD, K. and SASAKI, Y., 1998. Circulation, dense water formation, and outflow on the northeast Chukchi shelf. *Journal of Geophysical Research,* 103: 7647–7661.

WEFER, G. and BERGER, W. H., 1991. Isotope paleontology: growth and composition of extant calcareous species. *Marine Geology,* 100: 207–248.

WICKERT, A. D., 2016. Reconstruction of North American drainage basins and river discharge since the Last Glacial Maximum. *Earth Surface Dynamics,* 4: 831–869.

WILLIAMS, W. J. and CARMACK, E. C., 2015. The 'interior' shelves of the Arctic Ocean: Physical oceanographic setting, climatology and effects of sea-ice retreat on cross-shelf exchange. *Progress in Oceanography,* 139: 24–41.

WILLIAMS, W. J., MELLING, H., CARMACK, E. C. and INGRAM, R. G., 2008. Kugmallit Valley as a conduit for cross-shelf exchange on the Mackenzie shelf in the Beaufort Sea. *Journal of Geophysical Research,* 113: C02007, doi:10.1020/2006JC003591

WOOD, K. R., BOND, N. A., DANIELSON, S. L., OVERLAND, J. E., SALO, S. A., STABENO, P., et al., 2015. A decade of environmental change in the Pacific Arctic region. *Progress in Oceanography,* 136: 12–31.

XIA, J., ITO, E. and ENGSTROM, D. R., 1997a. Geochemistry of ostracode calcite: part 1. An experimental determination of oxygen isotope fractionation. *Geochimica et Cosmochimica Acta,* 61 (2): 377–382.

XIA, J., ENGSTROM, D. R. and ITO, E., 1997b. Geochemistry of ostracode calcite: part 2. The effects of water chemistry and seasonal temperature variation on *Candona rawsoni. Geochimica et Cosmochimica Acta,* 61 (2): 383–391.